Sum-Rate Maximization for RIS-Assisted Integrated Sensing and Communication Systems With Manifold Optimization

Eyad Shtaiwi, *Graduate Student Member, IEEE*, Hongliang Zhang, *Member, IEEE*, Ahmed Abdelhadi, *Senior Member, IEEE*, A. Lee Swindlehurst, *Fellow, IEEE*, Zhu Han, and H. Vincent Poor, *Life Fellow, IEEE*

***Abstract*— Integrated sensing and communication (ISAC) is a key enabler for next-generation wireless communication systems to improve spectral efficiency. However, the coexistence of sensing and communication functionalities can cause harmful interference. In this paper, we propose to use a reconfigurable intelligent surface (RIS) in conjunction with ISAC to address this issue. The RIS is composed of a large number of low-cost elements that can adjust the amplitude and phase shift of impinging signals, thus providing a relatively high beamforming gain. To maximize the sum-rate of the communication system, we jointly optimize the beamformer at the base station (BS) and the phase shifts at the RIS, subject to a threshold on the interference power, the unit-norm constraint of the transmit power, and the unit modulus constraint of the RIS phase shifts. To efficiently tackle this NP-hard problem, we first reformulate the problem into a more tractable form using the fractional programming (FP) technique. Then, we exploit the geometrical properties of the constraints and adopt an alternating manifold-based optimization to compute the optimal active beamformer and the RIS phase shifts, respectively. Simulation results demonstrate that the proposed RIS-assisted design significantly reduces the mutual interference and improves the system sum-rate for the communication system.**

***Index Terms*— Integrated sensing and communications, reconfigurable intelligent surface, sum-rate maximization, interference mitigation, manifold optimization.**

Manuscript received 29 September 2022; revised 31 March 2023; accepted 9 May 2023. Date of publication 22 May 2023; date of current version 16 August 2023. This work was supported by National Key R&D Project of China under Grant 2022YFE0111900; in part by the National Science Foundation under grant CNS-2107182 and ECCS-2030029; in part by NSF CNS-2107216, CNS-2128368, CMMI-2222810, US Department of Transportation, Toyota and Amazon; and in part by NSF under Grant CNS-2128448. The associate editor coordinating the review of this article and approving it for publication was S. Jin. *(Corresponding author: Eyad Shtaiwi.)*

Eyad Shtaiwi is with the Department of Electrical and Computer Engineering, University of Houston, Houston, TX 77004 USA (e-mail: emshtaiw@cougarnet.uh.edu).

Hongliang Zhang is with the School of Electronics, Peking University, Beijing 100871, China, and also with the Department of Electrical and Computer Engineering, Princeton University, Princeton, NJ 08544 USA.

Ahmed Abdelhadi is with the Department of Engineering Technology, University of Houston, Houston, TX 77004 USA.

A. Lee Swindlehurst is with the Center for Pervasive Communications and Computing, University of California at Irvine, Irvine, CA 92697 USA.

Zhu Han is with the Department of Electrical and Computer Engineering, University of Houston, Houston, TX 77004 USA, and also with the Department of Computer Science and Engineering, Kyung Hee University, Seoul 446-701, South Korea.

H. Vincent Poor is with the Department of Electrical and Computer Engineering, Princeton University, Princeton, NJ 08544 USA.

Color versions of one or more figures in this article are available at https://doi.org/10.1109/TCOMM.2023.3277872.

Digital Object Identifier 10.1109/TCOMM.2023.3277872

I. Introduction

NEXT-GENERATION communication systems are envisioned to integrate sensing and communication functions together. Such an integrated communication and sensing (ISAC) system enhances spectrum efficiency and reduces power consumption. A system that achieves radar and communication coexistence (RCC) is an example of ISAC. Most commercial communication systems have pushed towards higher operating frequencies and are accommodated in the sub-6 GHz band. Recently, a larger portion of the mmWave spectrum has been allocated for 5G deployments [1], [2]. On the other hand, radar remote sensing systems such as radar used for geophysical monitoring, air traffic control, weather observation, and surveillance for military applications primarily occupy a large portion of the same spectrum resources, e.g., the sub-6 GHz band. As a result, co-channel radar and communication systems will cause interference to each other [3], [4]. This has motivated joint radar and communications system designs, including proper spectrum sharing and interference mitigation algorithms, in order to achieve harmonious coexistence [5].

Recently, reconfigurable intelligent surface (RIS) technology has been received significant attention due to its capability for improving energy and spectrum efficiencies. An RIS consists of a large number of passive and low-cost elements that are capable of modifying the impinging electromagnetic (EM) signal's phase shift and amplitude. As a result, the RIS can customize the propagation environment to enhance signals of interest and suppress interference.

A. Related Work

Over the past decade, a plethora of spectrum-sharing approaches have been suggested to eliminate or mitigate the mutual interference between radar and communication systems for spectrum sharing. The major problem is to avoid harmful interference and guarantee satisfactory performance when both the radar and communication systems are simultaneously active. [11].

In [8], the authors considered a collocated Multiple-Input Multiple-Output (MIMO) radar and MIMO communication system based on matrix completion. The fusion center estimates the radar interference at the communication system user terminals (ComUT) and then subtracts it from the received

signals. However, this approach is not efficient in certain cases where the radar transmits with high power. Even when the power is not high, due to phase shift offsets between the radar transmitter and ComUTs, direct subtraction leaves residual interference. Therefore, this approach degrades the performance of the communication system. In [20], the authors proposed a signaling design to optimize the performance of both the radar and communication systems. The proposed design minimizes the mutual interference between the two systems and suppresses the interference between the multiple users of the communication system as well. However, the proposed approach is sensitive to noisy information such as bandwidth allocation, user types, and the number of spectrum users. The multi-objective optimization scheme is also difficult to generalize. The authors in [21], [22], and [24] considered cooperative design of the communication and radar waveforms to mitigate the mutual interference such that both systems work independently. While most of previous work focuses on the transmit beampattern design [1], [26], [27], [28], [29], [30], [31], [32], [33], [34] proposed receive beampattern designs that maximize the radar signal-to-interference-plus-noise ratio (SINR) subject to power constraints and a threshold on the rate of the communication system.

The authors in [36] considered a conventional MIMO radar system and MIMO communication system and proposed a joint precoding design of both the radar and communication transmitters over the same frequency. The precoding matrices were designed to maximize the mutual information and the SINR at the radar receiver with constraints on the signal-to-disturbance ratio (SDR), power budget, and data rate. Results showed that the optimized radar transmit precoder can mitigate clutter, reduce the radar interference at the ComUTs, and maximize the SINR at the radar receiver. The work in [40] proposed an interference management approach based on interference alignment (IA) for the RCC system. The authors proposed a joint precoder-decoder design by formulating an optimization problem that maximizes the SINRs of both the radar and the communication system. In [48], the authors studied the joint design of the communication transmit covariance matrix and the radar waveform to maximize the achievable rate for the communication system subject to energy constraints.

Dual-function radar communication (DFRC) systems were investigated in [41], [42], [43], [44], [45], and [46]. The authors of [41] proposed a RIS-assisted DFRC system to enhance the secrecy rate. The authors in [42], [45], and [46] proposed deployment of an RIS to improve target detection when a line-of-sight (LoS) signal path either does not exist or is weak. These papers considered DFRC systems where the RIS is deployed to enhance the radar performance. The DFRC requires an additional self-interference mitigation approach, unlike the separated radar and communication transmitters. In some situations (e.g., military applications), dual integration between the radar and communication systems is not allowed.

B. Contributions

In this paper, we propose a new scheme to improve the performance of multi-user (MU)-MIMO RCC systems by deploying an RIS. In this proposed approach, we exploit the beamforming capability of the RIS to mitigate the mutual interference between the communication and radar systems. Our approach aims to improve the performance of the communication system without interrupting the operation of the radar system. In particular, we study active beamforming at the base station (BS) and passive beamforming at the RIS to maximize the achievable sum-rate for the ComUTs while guaranteeing specific performance requirements for both systems.

We first formulate the sum-rate maximization problem based on the proposed system model. The formulated optimization problem is non-convex due to the non-convexity of both the objective function and the constraints. We use the fractional programming (FP) technique to transform the original problem into a more tractable form by introducing an auxiliary variable for each SINR [55]. Moreover, we exploit the differential properties of the constraints using manifold optimization. By exploiting the underlying geometries of the feasible set, the geometrical structures can deliver high-quality solutions to the NP-hard problem with a much lower computational cost. Therefore, we propose a manifold-based alternating optimization algorithm which tackles the beamformer designs directly on a Riemannian manifold [10]. Moreover, the optimization problem is reformulated as an unconstrained problem by establishing the geometrical structure of the feasible sets. The main contributions of this work are summarized as follows:

- We study an RIS-assisted MU-MIMO RCC system in which an RIS is leveraged to improve the sum-rate of the communication system. The proposed framework can mitigate the mutual interference (MUI) between the radar and communication systems. Our objective is to maximize the sum-rate for the ComUTs by jointly designing the active and passive beamforming at the BS and RIS, respectively, subject to the non-convex unit-norm power and the unit modulus constraints. This paper is one of the early attempts that address the sum-rate maximization for the RIS-aided MIMO RCC.
- We transform the formulated maximization problem into a simpler form using FP [55]. Then, we reformulate the constrained optimization problem into an unconstrained one by using the geometric properties of the constraints. Moreover, the unity modulus of the RIS phase shifts resembles a multiplication of multiple *complex unit circle manifolds*, while the search space for active beamforming lies in the *oblique manifold*.
- We propose a Riemannian conjugate gradient (RGC) method to solve the sum-rate maximization problem in the RIS-assisted MIMO RCC system. We provide a conjugate gradient (CG) method to optimize the active and passive beamformers that are replaced by complex unit circle and complex oblique manifolds. Specifically, we deploy the line search approach over *two manifolds*. Moreover, we divide the original problem into two sub-problems over two different manifolds. We re-express the objective functions in such a way that we are able to compute the Riemannian gradients.
- Our simulation results demonstrate that the RIS is beneficial in improving the sum-rate performance for the

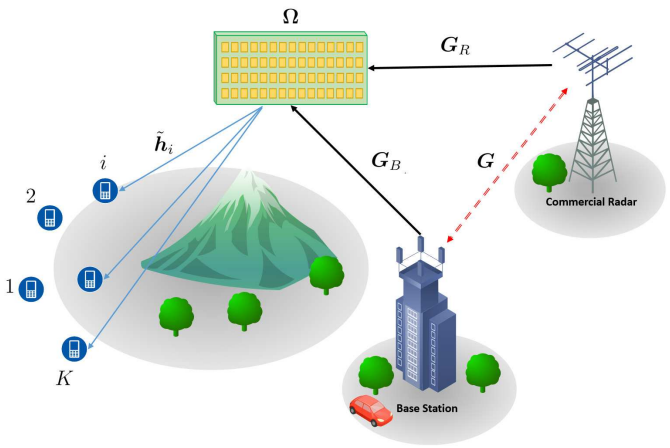

Fig. 1. RIS-assisted MIMO RCC system.

communication system and reducing the interference from the BS to the radar system. In particular, numerical simulations show the advantages of RIS-assisted ISAC in improving the communication system sum-rate and mitigating the mutual interference between both systems.

In our earlier conference paper [52], we presented the RIS-assisted RCC system framework and proposed a simple local search approach to optimize the beamforming at the BS and the RIS phase shifts.

C. Organization and Notation

The rest of this paper is organized as follows. Section II presents the system model of our assumed RIS-assisted MIMO RCC system. In Section III, we discuss the performance metric of interest and formulate the design problem. Then, we introduce the proposed algorithm to jointly optimize the active and passive beamforming in Section IV. Section V presents numerical results to demonstrate the performance of our proposed approach and its effectiveness. Finally, Section VI concludes the paper.

***Notations*:** Throughout this paper, scalars are denoted by lower-case letters. Bold lower case letters and bold upper-case letters denote vectors and matrices, respectively. A calligraphy upper-case letter represents a set. For a vector $\mathbf{x}$, $||\mathbf{x}||^2$ defines its Euclidean norm and $\mathbf{x}^\dagger$ represents its conjugate transpose. $\mathbf{I}_N$ denotes an $N \times N$ identity matrix. The symbols $(\cdot)^T$, $(\cdot)^*$ and $(\cdot)^H$ denote transpose, conjugate, and Hermitian transpose, respectively. The operator $\mathrm{vec}(\cdot)$ stacks the columns of a matrix to construct a vector, $\mathrm{tr}(\cdot)$ represents the trace of a matrix, $\mathbf{0}_N$ denotes the N-dimensional zero vector, $\mathrm{diag}(\mathbf{A})$ extracts the diagonal elements of matrix $\mathbf{A}$ to construct a vector, $\mathbf{1}$ indicates the all-ones vector, $|\mathbf{a}|$ denotes the modulus of $\mathbf{a}$, $\otimes$ and $\odot$ denote the Kronecker product and the Hadamard product, respectively, and $\mathfrak{Re}\{\mathbf{x}\}$ indicates the element-wise real part of $\mathbf{x}$.

II. System Model

In this paper, we propose an RIS-assisted MIMO RCC system as shown in Fig. 1. Specifically, we consider a time division duplex (TDD) downlink system that includes a BS, an RIS, a MIMO radar, and multiple single-antenna users (UEs). Here, the RIS is deployed to improve the received SINR and reduce the mutual interference. We assume a quasi-static flat fading channel model where the channel varies independently among coherence blocks and remains constant within the transmission block. We also assume that a central control unit links the BS, the RIS, and the radar, and thus the channel information for all links is available at the BS and the radar [12].

In this work, we assume that line-of-sight (LOS) paths between the BS and UEs and between the radar transmitter and UEs are not available. The BS is equipped with M antenna elements, and the RIS has N reflecting elements. The BS and the radar share the same frequency spectrum. In this paper, we consider a collocated MIMO radar with with L_t and L_r transmitting and receiving antennas, respectively, so that the Angle-of-Arrival and the Angle-of-Departure are the same [6]. The collocated MIMO radar has a uniform linear array (ULA) configuration with elements spacing on the order of the half the wavelength. The collocated MIMO radar is widely used since it gives better target parameter identification and spatial resolution. Moreover, for the radar target, we adopt a point target model where the target's scatterer an infinitesimal spatial extent [7]. The point target model is considered a good assumption and has been widely used in the radar theory especially for collocated MIMO radar cases when the target is located in the far-filed of the radar array, i.e., there are a large distance between the radar and the target compared to the elements inter-spacing distance. For simplicity and without loss of generality, we assume $L_t = L_r = L_R$.

The RIS can be modeled using a diagonal matrix $\mathbf{\Omega} = diag(\omega_1, \omega_2, \ldots, \omega_N)$ where the reflection coefficient $\omega_i = A_i e^{j\Omega_i}$ comprises an amplitude coefficient $A_i \in (0, 1]$, and a phase coefficient $\Omega_i \in [0, 2\pi]$. In order to exploit the maximum reflection capability of the RIS, the amplitude coefficients in this work are set to 1, i.e., $A_i = 1$ [50].

The channel between the K ComUTs and the RIS is $\mathbf{H}_t = \left[\tilde{\mathbf{h}}_1, \tilde{\mathbf{h}}_2, \cdots, \tilde{\mathbf{h}}_K\right]^T \in \mathcal{C}^{K\times N}$ with $\tilde{\mathbf{h}}_i^H \in \mathcal{C}^{N\times 1}$ being the channel vector between the RIS and the i^{th} UE. $\mathbf{G}_B \in \mathcal{C}^{N\times M}$ and $\mathbf{G}_R \in \mathcal{C}^{N\times L_R}$ are channels between the RIS and the BS, and the RIS and radar, respectively. Let $\mathbf{H}_c = [\mathbf{h}_1, \mathbf{h}_2, \cdots, \mathbf{h}_K]^T \in \mathcal{C}^{K\times M}$ represent the cascaded channel from the BS to these K UEs via the RIS. Here, $\mathbf{h}_i = \tilde{\mathbf{h}}_i \mathbf{\Omega} \mathbf{G}_B \in \mathcal{C}^{1\times M}$ represents the communication channel vector between the BS and the i^{th} UE via the RIS. In addition, the cascaded channel between the radar transmitter and the UEs is denoted as $\mathbf{F}_c = \left[\tilde{\mathbf{f}}_1, \tilde{\mathbf{f}}_2, \cdots, \tilde{\mathbf{f}}_K\right]^T \in \mathcal{C}^{K\times L_R}$ with $\tilde{\mathbf{f}}_i = \tilde{\mathbf{h}}_i \mathbf{\Omega} \mathbf{G}_R \in \mathcal{C}^{1\times L_R}$ denoting the interference channel vector from the radar transmitter to the i^{th} ComUT. Moreover, the interfering channel between the BS and Radar is $\mathbf{G} = [\mathbf{g}_1, \mathbf{g}_2, \ldots, \mathbf{g}_M] \in \mathcal{C}^{L\times M}$. Since both the BS and the radar system operate on the same frequency resource, the received signal at the i^{th} UE is expressed as [37]

$$y_i^c[l] = \mathbf{h}_i \sum_{k=1}^{K} \mathbf{w}_k s_k[l] + \sqrt{P_R}\tilde{\mathbf{f}}_i \mathbf{s}_l + n_i[l], i = 1, 2, \ldots, K, \quad (1)$$

where $\mathbf{w}_k$ and $s_k[l]$ are the beamforming vector and the transmitted symbol to the k^{th} UE at time l, where $l = \{1, 2, \ldots, T\}$ and T denotes the communication frame length. The received noise at the i^{th} UE is $n_i[l] \sim \mathcal{CN}(0, \sigma_c^2)$. The radar transmitter has a total transmit power budget P_R, and $\mathbf{s}_l$ represents the orthogonal waveforms used by the radar system, i.e., $\frac{1}{L_o}\sum_{l=1}^{L_o} \mathbf{s}_l\mathbf{s}_l^H = \mathbf{I}$, where L_o represents the communication system frame length. Without loss of generality, we assume that each column of the beamforming matrix has a unit norm such that the beamforming vector for the k^{th} user satisfies $||\mathbf{w}_k||^2 = 1$, $\forall k \in \{1, 2, \cdots, K\}$.

After compensating the range-Doppler parameters, the signal received from a single point target at an angle θ, in the far-field with constant radial velocity and in a single range-Doppler bin of the radar is given by [35] and [56]

$$\mathbf{y}_l^R = \alpha\sqrt{P_R}\mathbf{a}_R(\theta)\mathbf{a}_T^T(\theta)s_l + \left(\mathbf{G}_R^H\mathbf{\Omega}\mathbf{G}_B + \mathbf{G}^H\right)\sum_{k=1}^{K}\mathbf{w}_k d_k[l] + \mathbf{n}_l, \quad (2)$$

$$\triangleq \alpha\sqrt{P_R}\mathbf{A}(\theta)s_l + \tilde{\mathbf{G}}\sum_{k=1}^{K}\mathbf{w}_k d_k[l] + \mathbf{n}_l, \quad (3)$$

where α, $\mathbf{n}_l = [\mathrm{n}_1[l], \mathrm{n}_2[l], \ldots, \mathrm{n}_M[l]]^T$, $\mathbf{a}_R$, $\mathbf{a}_T$, and $\tilde{\mathbf{G}} = [\tilde{\mathbf{g}}_1, \tilde{\mathbf{g}}_2, \ldots, \tilde{\mathbf{g}}_M] \in \mathcal{C}^{L\times M}$ are the complex path-loss, the received noise vector at the l-time index, the receive steering vector, the transmit steering vector, and the cascaded interference channel matrix between the BS and the radar receiver, respectively. α and θ are unknown deterministic parameters represent the complex amplitude and the direction of arrival of the target, respectively. Specifically, the angle θ represents the azimuth angle of the point target. Due to the far-field assumptions, α is assumed to identical for the receive and transmit array. In this paper, we use the Saleh-Valenzuela channel model in which the wireless channel is characterized using the parameters of the multipath components which include complex path losses, delays, angle-of-arrivals, and angle-of-departures [9], [57], [58]. Therefore, the channel between any two nodes in the system is assumed to be described as

$$\mathbf{H}_{\text{gen}} = \sqrt{\frac{\mu_t\mu_r}{\Upsilon_n}}\sum_{\upsilon_n=0}^{\Upsilon_n}\kappa_{\upsilon_n}\mathbf{\Lambda}_t\left(\theta^{\upsilon_n}, \phi^{\upsilon_n}\right)\mathbf{\Lambda}_r^T\left(\theta^{\upsilon_n}, \phi^{\upsilon_n}\right), \quad (4)$$

where μ_t and μ_r are the numbers of antennas at the transmitter and receiver, respectively. The number of sub-paths between the transmitter and receiver is denoted by Υ_n, while κ_{υ_n} represents the pathloss of the ${\upsilon_n}^{th}$ path. In addition, the steering vectors of the transmitter and the receiver arrays are given by $\mathbf{\Lambda}_t\left(\theta^{\upsilon_n}, \phi^{\upsilon_n}\right)$ and $\mathbf{\Lambda}_r\left(\theta^{\upsilon_n}, \phi^{\upsilon_n}\right)$, with θ^{υ_n} and ϕ^{υ_n} representing the azimuth and elevation angles of arrival and departure of the ${\upsilon_n}^{th}$ subpath, respectively [13]. The steering vectors are a function of the carrier wavelength λ and the antenna array configuration. In this paper, we consider uniform linear array and uniform planar array structures. The steering vector for a uniform planar array with N_1 and N_2 on the horizontal and vertical axes, respectively, can be expressed as $\mathbf{a}_{\text{UPA}}(\theta, \phi) = \frac{1}{\sqrt{N_1N_2}}[1, \ldots, e^{jkd(m\sin(\theta)\sin(\phi)+n\cos(\phi))}, \ldots, e^{jkd((N_1-1)\sin(\theta)\sin(\phi)+(N_2-1)\cos(\phi))}]^T$, where d is the inter-element spacing, $0 \le m < N_1$ and $0 \le n < N_2$ are the antenna element indices and the antenna array size is N_1N_2, and $k = 2\pi/\lambda$ [14]. For an N_{ULA}-element uniform linear array, the steering vector can be expressed as $\mathbf{a}_{\text{ULA}}(\theta) = \frac{1}{\sqrt{N_{ULA}}}\left[1, e^{jkd\sin(\theta)}, \ldots, e^{j(N_{ULA}-1)kd\sin(\theta)}\right]^T$. Note that the steering vector of the uniform linear array structure is invariant in the elevation angle, therefore, we do not include ϕ. Furthermore, we assume that the inter-element spacing for the arrays is equal to $\lambda/2$, and therefore, the channels among different antenna elements are independent [15]. We also assume the channel vectors, i.e., $\tilde{\mathbf{h}}_i$ $\forall i \in \{1, 2, \cdots, K\}$, are modeled as complex Gaussian since the ComUTs are equipped with omni-directional antennas.

In this paper, we rely on the following assumptions:

1) We ignore the interference caused by false targets and clutter [37]. Therefore, the communication system is the only source of interference in the radar system [4], [16], [17], [18], [19].
2) The channel state information (CSI) is assumed to be known at the BS. For the communication system, there are several techniques to estimate the channels. The authors in [62] proposed an approach that exploits the properties of symmetric positive definite matrices. Similarly, the interference channels can be computed by assuming coordination between both the radar and BS [64]. Equivalently, the acquisition of the CSI of the interference channels can be performed by radar fusion or coordination center.
3) The duration for a communication system symbol is the same as the duration of the sub-pulse of the radar system. This assumption is valid in practical scenarios; for example, the symbol duration for LTE systems and the S-band radar sub-pulse duration are the same [8].
4) The radar transmit waveforms, i.e., $\mathbf{S} = [\mathbf{s}_1, \mathbf{s}_2, \ldots, \mathbf{s}_L]$, are set to be orthogonal according to assumptions in the collocated MIMO radar literature [35]. In other words, the coherence matrix of the baseband equivalent signals is given by

$$\mathbf{R}_{\mathbf{s}} = \frac{1}{L_o}\sum_{l=1}^{L_o}\mathbf{s}[l]\mathbf{s}^H[l] = \begin{bmatrix} 1 & \beta_{12} & \cdots & \beta_{1L} \\ \beta_{21} & 1 & \cdots & \beta_{2L} \\ \vdots & \vdots & \ddots & \vdots \\ \beta_{L1} & \beta_{L2} & \cdots & 1 \end{bmatrix}, \quad (5)$$

   where l, and $\beta_{n'k'}$ represent the time index and the complex correlation coefficient between the n'^{th} and the k'^{th} signals, respectively. The phases of $\beta_{n'k'}\forall n', k' = 1, 2, \ldots, L$ modify the beam direction of the coherent component of the transmitted signals. In this paper, we assume that $\beta_{n'k'} = 0, n' \neq k'$ and the coherence matrix is an identity matrix, i.e., $\mathbf{R}_{\mathbf{s}} = \mathbf{I}$.
5) The channels $\mathbf{H}_t$, $\mathbf{F}_c$, and $\tilde{\mathbf{G}}$ are flat Rayleigh fading and are assumed to be statistically independent, and the radar signals are statistically independent of the communication signals [3], [4], [8], [23].

In the rest of the paper, we omit the time index l for convenience unless otherwise mentioned.

III. Problem Formulation

In this section, we formulate a sum-rate maximization problem for the proposed RIS-assisted RCC system. We aim to select the optimal phase shifts for the RIS elements and the beamformer at the BS to not only maximize the sum rate for the communication system, but also mitigate the interference between the radar and the communication systems. To be specific, the optimal phase shifts matrix and the beamforming vectors need to meet the following requirements:

- Eliminate the mutual interference between the communication and the radar system by maintaining the interfering power from the communication system to be below a certain threshold $\hat{p_0}$.
- Maintain the transmit power within the budget for both the radar transmitter and the BS. We investigate active and passive beamforming designs for the BS and RIS, respectively, focusing on optimization of the communication system performance metric. In this paper, we aim to maximize the sum-rate under the constraints of the total transmit power for the communication system.

Under the aforementioned assumptions and based on the system model in (1) and (3), the received (SINR) at the i^{th} ComUT which is denoted by ρ_i can be expressed as

$$\begin{aligned}\rho_i &= \frac{|\mathbf{h}_i^H \mathbf{w}_i|^2}{\sum\limits_{k=1,k\neq i}^{K} |\mathbf{h}_i^H \mathbf{w}_k|^2 + P_R\|\mathbf{f}_i\|^2 + \sigma_c^2} \\ &= \frac{\mathrm{tr}\left(\mathbf{h}_i^* \mathbf{h}_i^T \mathbf{W}_i\right)}{\mathrm{tr}\left(\mathbf{h}_i^* \mathbf{h}_i^T \sum\limits_{\substack{k=1\\k\neq i}}^{K} \mathbf{W}_k\right) + \mathrm{tr}\left(\mathbf{f}_i^* \mathbf{f}_i^T P_R\right) + \sigma_c^2},\end{aligned} \tag{6}$$

where $\mathbf{W}_i = \mathbf{w}_i \mathbf{w}_i^H$. Therefore, the normalized achievable sum-rate of the communication system assuming that all ComUTs utilize the same bandwidth is given by

$$R = \frac{C}{B} = \sum_{i=1}^{K} \log_2(1+\rho_i), \tag{7}$$

where B and C denote the available spectrum bandwidth and the system capacity, respectively. The main challenge for the coexistence design is to eliminate the mutual interference between the two systems. The interference power of the BS transmission on the radar system can be expressed as

$$\begin{aligned}P_{int} &= \sum_{m=1}^{L} \left| \tilde{\mathbf{g}}_m^T \sum_{k=1}^{K} \mathbf{w}_k \right|^2 \\ &= \sum_{m=1}^{L} tr\left(\tilde{\mathbf{g}}_m^* \tilde{\mathbf{g}}_m^T \sum_{k=1}^{K} \mathbf{w}_k \mathbf{w}_k^H \right) = tr\left(\tilde{\mathbf{G}}^* \tilde{\mathbf{G}}^T \mathbf{\Pi}_c \right),\end{aligned} \tag{8}$$

where $\mathbf{\Pi}_c = \sum\limits_{k=1}^{K} \mathbf{w}_k \mathbf{w}_k^H$. Since we consider a downlink scenario, the ComUTs will not transmit interfering signals to the radar receiver. Therefore, the BS is the only source of interference to the radar system. The optimization problem that maximizes the overall achievable rate R for the communication system and meets the transmit power and BS interference power constraints is formulated as

$$\underset{\{\mathbf{w}_k\},\mathbf{\Omega}}{\text{maximize}}\ R = \sum_{i=1}^{K} \log_2(1+\rho_i) \tag{9a}$$

$$\text{subject to}\quad |\omega_n| = 1, \forall n = 1,\ldots,N \tag{9b}$$

$$P_{int} \leq \hat{p_0} \tag{9c}$$

$$||\mathbf{w}_k||^2 = 1 \tag{9d}$$

$$P_k \leq \tfrac{P_C}{K}, \forall k \in \mathcal{K}, \tag{9e}$$

where $\hat{p_0}$ is the maximum tolerable interference-to-noise ratio at the radar receiver from the communication BS. The constraint (9e) denotes the total transmit communication system power where P_C represents the budget of the communication BS transmit power consumption and P_k is the average transmit power for each communication system user.

It can be easily noted that problem (9a) is non-convex due to the existence of the interference, and thus finding the solution is challenging. Fortunately, the fractional programming (FP) technique can translate (9a) into a more tractable form [55]. The FP approach applies the Lagrangian dual transform techniques to move the SINR ratio, i.e., ρ_i, outside the logarithm function. The transformation is done by introducing an auxiliary variable and is capable of converting (9a) into a sum-of-ratios form described by

$$\underset{\mathbf{W},\mathbf{\Omega},\ \nu}{\text{maximize}}\ \mathcal{L}\left(\mathbf{w}_k, \mathbf{\Omega}, \nu\right)$$

$$\text{subject to}\quad (9b) - (9e), \tag{10a}$$

where $\nu = \{\nu_1, \cdots, \nu_K\}$ and ν_i is the introduced auxiliary variable for each SINR ratio ρ_i. Here, the new objective function $\mathcal{L}\left(\mathbf{w}_k, \mathbf{\Omega}, \nu\right)$ is given by

$$\begin{aligned}\mathcal{L}\left(\mathbf{W}, \mathbf{\Omega}, \nu\right) = &\sum_{i=1}^{K} \log\left(1+\nu_i\right) - \sum_{i=1}^{K} \nu_i \\ &+ \underbrace{\sum_{i=1}^{K} \frac{(1+\nu_i) A_i(\mathbf{W}, \mathbf{\Omega})}{A_i(\mathbf{W}, \mathbf{\Omega}) + B_i(\mathbf{W}, \mathbf{\Omega})}}_{\text{Sum-of-ratio term}},\end{aligned} \tag{11}$$

where $\rho_i = \frac{A_i(\mathbf{W},\mathbf{\Omega})}{B_i(\mathbf{W},\mathbf{\Omega})}$. The following proposition shows that the transformed and original problems have the same solution.

Proposition 1: The two problems in (9a) and (10a) are equivalent in the sense that $\{\mathbf{W}, \mathbf{\Omega}\}$ are the solution to (9a) if and only if they are the solution to (10a), and the optimal objective values of these two problems are also equal.

Proof: For fixed $\mathbf{w_k}, \mathbf{\Omega}$, the new objective function is a concave and differentiable function over ν, therefore, the optimal ν can be determined by setting $\partial\mathcal{L}/\partial\nu_i$ to zero, $\forall i$, i.e., $\nu_i^\star = \rho_i$ [55]. □

Therefore, for a fixed ν, problem (10a) is equivalent to

$$\underset{\mathbf{W},\mathbf{\Omega}}{\text{maximize}}\quad \tilde{\mathcal{L}}_1\left(\mathbf{W}, \mathbf{\Omega}\right)$$

$$\text{subject to}\quad (9b) - (9e), \tag{12a}$$

where

$$\tilde{\mathcal{L}}_1(\mathbf{W},\mathbf{\Omega}) = \sum_{i=1}^{K} \frac{(1+\nu_i)|\mathbf{h}_i^H\mathbf{w}_i|^2}{\sum\limits_{k=1}^{K}|\mathbf{h}_i^H\mathbf{w}_k|^2 + P_R\|\mathbf{f}_i\|^2 + \sigma_c^2}.$$

To simplify, we incorporate the interfering power constraint (9c) into the objective function as a penalty term. The penalty-based approach approximates the constrained optimization problem by incorporating some or all the constraints to the objective function as a penalty term [60], [61]. Penalizing the constraints forces the infeasible points to get relatively high cost compared to the feasible points, and force the optimizer to get closer to the feasible points. It has been proven that the original problem and the penalty problem are equivalent. Specifically, we add the square error between the interfering power and the threshold, i.e., sum-square penalty, to the objective function. The sum-square penalty is computed as [59]

$$\lambda(P_{int}) = (\hat{p}_0 - P_{int})^2 = \left(\hat{p}_0 - tr\left(\tilde{\mathbf{G}}^*\tilde{\mathbf{G}}^T\mathbf{\Pi}_c\right)\right)^2. \quad (13)$$

Therefore, (12a) can be reformulated as

$$\underset{\mathbf{W},\mathbf{\Omega}}{\text{maximize}} \quad \mathcal{L}_1(\mathbf{W},\mathbf{\Omega}) \quad (14a)$$

$$\text{subject to} \quad (9b), (9d), (9e), \quad (14b)$$

where $\mathcal{L}_1(\mathbf{W},\mathbf{\Omega}) = \tilde{\mathcal{L}}_1(\mathbf{W},\mathbf{\Omega}) - \lambda(P_{int}) = \tilde{\mathcal{L}}_1(\mathbf{W},\mathbf{\Omega}) - ||\hat{p}_0 - tr\left(\tilde{\mathbf{G}}^*\tilde{\mathbf{G}}^T\mathbf{\Pi}_c\right)||^2$.

The optimization problem in (14a) is non-convex, because of the coupling between the optimization parameters in (9b) and (9d). To address this issue, we first decouple the constraints in (9b) and (9d) and optimize in an alternating matter. Specifically, we decouple the beamforming at the BS and the RIS phase shifts by optimizing one variable at a time assuming the other one is fixed. Moreover, we first fixed the active beamforming matrix at the BS to optimize the RIS passive beamforming by solving (15a). After obtaining the optimal RIS phase shifts, we optimize the active beamforming at the BS by assuming the RIS phase shifts is given by (16a). The procedures continue until convergence.

In subsections IV-A and IV-B, we provide methods to find the optimal solution $\mathbf{\Omega}^*$ by fixing $\mathbf{W}$, and then find the solution $\mathbf{W}^*$ by fixing $\mathbf{\Omega}$ by exploiting the differential geometry of the constraints. This manifold-based optimization approach has shown advantages over conventional optimization techniques in terms of computational and spectral efficiencies. Moreover, the low-dimentionality feature of the smooth manifolds helps to efficiently solve the non-convex problem. Next, we will provide a preliminary introduction for the readers on manifold optimization.

Optimizations on manifolds have been studied extensively during the last decade [51]. Exploiting the differentiable geometries of the constraints can deliver much lower computational costs and high quality solutions for NP-hard problems. Therefore, we propose algorithms using alternating manifold optimization (AMO) which tackles the optimization problem directly on Riemannian manifolds and sub-manifolds. We view the feasible set for the optimization problem as Riemannian manifolds in particular the complex circle manifold and the oblique manifold. The active transmit beamforming and the RIS phase shifts of the constrained optimization problem are reformulated as an unconstrained problem using the aforementioned manifolds. Instead of using algorithms on Euclidean space, we provide gradient ascent, and conjugate-gradient methods to solve the optimization problem using the Riemannian trust-region method.

A. Problem Reformulation

We employ alternating optimization to solve (14a). Specifically, for a fixed value for the auxiliary variable, i.e., $\nu_i^\star = \rho_i$, (14b) can be solved iteratively by fixing $\mathbf{W}$ and solving for $\mathbf{\Omega}$, and in the next phase, the solution $\mathbf{W}$ is obtained by fixing $\mathbf{\Omega}$. The power allocation can be easily performed using [25], thus constraint (9e) can be neglected. Consequently, (12a) is transformed to the following two optimization problems

$$\underset{\mathbf{\Omega}}{\text{maximize}} \quad f_1(\mathbf{\Omega}) \quad (15a)$$

$$\text{subject to} \quad (9b), \quad (15b)$$

and

$$\underset{\mathbf{W}}{\text{maximize}} \quad f_2(\mathbf{W}) \quad (16a)$$

$$\text{subject to} \quad (9d), \quad (16b)$$

where expressions for $f_1(\mathbf{\Omega})$ and $f_2(\mathbf{W})$ will be given later. For ease of presentation, let $\mathbf{q} = [e^{-j\omega_1}, \cdots, e^{-j\omega_N}] \in \mathbb{C}^{1\times N}$. Therefore, channels $\mathbf{h}_i$ and $\tilde{\mathbf{f}}_i$ can be re-written as

$$\mathbf{h}_i = \mathbf{q}\text{diag}(\tilde{\mathbf{h}}_i)\mathbf{G}_B = \mathbf{q}\mathbf{\Upsilon}_{Bi} \in \mathcal{C}^{1\times M}, \quad (17)$$

$$\mathbf{f}_i = \mathbf{q}\text{diag}(\tilde{\mathbf{h}}_i)\mathbf{G}_R = \mathbf{q}\mathbf{\Upsilon}_{Ri} \in \mathcal{C}^{1\times L_R}. \quad (18)$$

Substituting (17) and (18) in (12a) yields

$$f_1(\mathbf{\Omega}) = \sum_{i=1}^{K} \frac{(1+\nu_i)|\mathbf{q}\varsigma_{i,i}|^2}{\sum\limits_{k=1}^{K}|\mathbf{q}\varsigma_{i,k}|^2 + P_R\|\mathbf{q}\mathbf{\Upsilon}_{Ri}\|^2 + \sigma_c^2} - \lambda(P_{int}), \quad (19)$$

where $\varsigma_{i,k} = \mathbf{\Upsilon}_{Bi}\mathbf{w}_k$, and

$$f_2(\mathbf{W}) = \sum_{i=1}^{K} \frac{(1+\nu_i)|\mathbf{h}_i^H\mathbf{W}\upsilon_i|^2}{\sum\limits_{k=1}^{K}|\mathbf{h}_i^H\mathbf{W}\upsilon_k|^2 + P_R\|\mathbf{f}_i\|^2 + \sigma_c^2} - \lambda(P_{int}), \quad (20)$$

where $\mathbf{W} = [\mathbf{w_1}, \mathbf{w}_2, \cdots, \mathbf{w}_K] \in \mathbb{C}^{M\times K}$, and $\upsilon_i = [\mathbb{I}_K]_i$ is the i^{th} column of an identity matrix. such that $\mathbf{W}\upsilon_k = \mathbf{w}_k$.

Next, we provide the Euclidean gradients of both objective functions, $f_1(\mathbf{\Omega})$ and $f_2(\mathbf{W})$ in (21) and (22), as shown at the bottom of the next page, respectively.

IV. The Proposed Approach

In this section, a manifold-based optimization approach is developed to solve (15a) and (16a), respectively. Applying manifold optimization achieves a good balance between performance and the computational complexity. The basic principle of the concept behind AMO approaches is to reformulate

the problem as an unconstrained problem over the manifold instead of performing the optimization on the ambient Euclidean space. In the following subsections, we introduce two methods to solve (15a) and (16a) using a line search over the two manifolds, respectively.

A. Phase 1: RMO-Based RIS Phase Shifts Design

In this subsection, we propose a *Reimannian Manifold Optimization* (RMO) to solve the problem formulated in (15a). Due to the constant modulus constraint (CMC), the problem is well-known to be an NP-hard problem. Note that other approaches such as the monotonically error-bound improving technique (MERIT), semi-definite relaxation with randomization (SDR), and the majorization-minimization framework could also be used. Some of these methods require relatively high computational cost due to the presence of the non-convex CMC.

The geometrical structure of the CMC in (15a) allows formulation of a Riemannian manifold or sub-manifold that transforms the constrained optimization problem into unconstrained one. Then, line search methods can be applied on the manifolds instead of the ambient Euclidean space. To find the unconstrained gradient-based optimization algorithm on Riemannian manifolds, we first reformulate (16a) into the following unconstrained problem [38]

$$\underset{\boldsymbol{\Omega}\in\mathcal{M}}{\text{maximize}}\; f_1\left(\boldsymbol{\Omega}\right), \tag{23a}$$

where $\mathcal{M}$ is the Riemannian manifold that defines the constraint for the problem (15a).

The optimal solution for (15a) can be viewed as a search of a product over N complex circles. In other words, the feasible search space of the original problem can be considered as

$$\underbrace{\mathcal{S}\times\mathcal{S}\cdots\times\mathcal{S}}_{N\ \text{times}} \tag{24}$$

where $\mathcal{S}$ is a complex circle defined as $\mathcal{S}\triangleq\{\omega_i\in\mathbb{C}:{\omega_i}^*\omega_i=\text{Re}\{\omega_i\}^2+\text{Im}\{\omega_i\}^2=1\}$. The set $\mathcal{S}$ can be thought of as a Riemannian sub-manifold of $\mathbb{C}$, and therefore, the product of multiple complex circles in (24) is a sub-manifold of $\mathbb{C}^N$. Thus, the feasible set of the N RIS reflection coefficients is itself a smooth Riemannian sub-manifold of $\mathbb{C}^N$ and known as the *complex circle manifold* (CCM), and is defined as [39]

$$\mathcal{S}^N\triangleq\{\omega\in\mathbb{C}^N:|\omega_l|=1,\ l=1,2,\ldots,N\}. \tag{25}$$

The proposed approach applies gradient ascent on $\mathcal{S}^N$ which is similar to that on the ambient Euclidean space.

The proposed approach consists of two phases, namely, evaluating the ascent direction by finding the Riemannian gradient of the current solution, then increasing the objective function using the line search until a stopping criteria is met.

Since the gradient ascent is performed on the CCM, the search direction will be computed on the manifold, i.e., $\mathcal{S}^N$, itself rather than in the ambient Euclidean space. Consequently, the search direction is determined by the Riemannian, or intrinsic, gradient of the objective function. Computing the Riemannian gradient requires the tangent space which consists of a set of all the vectors tangent to the manifold. The tangent space to the CCM admits a closed-form formula as follows

$$\mathcal{T}_{\boldsymbol{\Gamma}_{(i)}}\mathcal{S}^L=\left\{\boldsymbol{\eta}\in\mathbb{C}^{L+1}\ :\ \text{Re}\left\{\boldsymbol{\eta}^*\odot\boldsymbol{\Gamma}_{(i)}\right\}=\mathbf{0}\right\}. \tag{26}$$

The Riemannian gradient of $f_1(\boldsymbol{\Omega})$ at a point $\boldsymbol{\Gamma}_{(k)}\in\mathcal{S}^N=\mathcal{M}$ is $\nabla_{\mathcal{M}}f_1(\boldsymbol{\Gamma}_{(k)})$, which represents a vector in the tangent space. For the CCM, the Riemannian gradient is computed by the projection of the conventional gradient onto the tangent space by a projection operator $\mathbf{P}_{\mathcal{T}_{\boldsymbol{\Gamma}_{(k)}}\mathcal{M}}(\nabla_{\mathcal{M}}f_1(\boldsymbol{\Gamma}_{(k)}))$.

The computation of the projection for the CCM is derived from those for the (real) unit circle manifold which is defined by $\mathcal{C}^1\triangleq\{\mathbf{q}\in\mathbb{R}^2:\mathbf{q}^T\mathbf{q}=1\}$. The projection of a vector

$$\begin{aligned}\nabla_{\mathbf{q}}f_1\left(\boldsymbol{\Omega}\right)=&\sum_{i=1}^{K}(1+\nu_i)\left\{\frac{2\varsigma_{i,i}^H\mathbf{q}\varsigma_{i,i}}{\sum\limits_{k=1}^{K}|\mathbf{q}\varsigma_{i,k}|^2+P_R\|\mathbf{q}\boldsymbol{\Upsilon}_{Ri}\|^2+\sigma_c^2}-2\sum_{s=1}^{K}\frac{2|\mathbf{q}\varsigma_{i,i}|^2\left(\varsigma_{i,s}^H\mathbf{q}\varsigma_{i,s}+2P_R(\mathbf{q}\boldsymbol{\Upsilon}_{Ri})^H\boldsymbol{\Upsilon}_{Ri}^H\right)}{\left(\sum\limits_{k=1}^{K}|\mathbf{q}\varsigma_{i,k}|^2+P_R\|\mathbf{q}\boldsymbol{\Upsilon}_{Ri}\|^2+\sigma_c^2\right)^2}\right\}\\&+4\sum_{i=1}^{L_R}\left(\hat{p}_0-tr\left(\tilde{\mathbf{G}}^*\tilde{\mathbf{G}}^T\boldsymbol{\Pi}_c\right)\right)\left(\left(\mathbf{q}\left(\text{diag}(\mathbf{g}_{rr,i}^H)^*\mathbf{G}_B^*\mathbf{G}_B^T\text{diag}(\mathbf{g}_{rr,i}^H)\text{diag}(\mathbf{g}_{rr,i}^H)\mathbf{G}_B\mathbf{G}_B^H\text{diag}(\mathbf{g}_{rr,i})\right)\right)\right.\\&\left.\mathbf{g}_i^*\mathbf{G}_B^T\text{diag}(\mathbf{g}_{rr,i}^H)\right)\boldsymbol{\Pi}_c+\mathbf{g}_i\mathbf{G}_B^H*\text{diag}(\mathbf{g}_{rr,i})\boldsymbol{\Pi}_c.\end{aligned} \tag{21}$$

$$\begin{aligned}\nabla_{\mathbf{W}}f_2\left(\mathbf{W}\right)=&\sum_{i=1}^{K}(1+\nu_i)\left\{\frac{2\mathbf{h}_i^H\upsilon_i\mathbf{W}\mathbf{h}_i\upsilon_i^H}{\sum\limits_{k=1}^{K}|\mathbf{h}_i^H\mathbf{W}\upsilon_k|^2+P_R\|\mathbf{f}_i\|^2+\sigma_c^2}-2\sum_{s=1}^{K}\frac{2|\mathbf{h}_i^H\mathbf{W}\upsilon_i|^2\mathbf{h}_i^H\upsilon_s\mathbf{W}\mathbf{h}_i\upsilon_s^H}{\left(\sum\limits_{k=1}^{K}|\mathbf{h}_i^H\mathbf{W}\upsilon_k|^2+P_R\|\mathbf{f}_i\|^2+\sigma_c^2\right)^2}\right\}\\&+4\sum_{l=1}^{L_R}\left(\hat{p}_0-\tilde{g}_l\mathbf{W}\mathbf{1}_K\mathbf{1}_K^\top\tilde{g}_l^H\right)\tilde{g}_l\tilde{g}_l^H\mathbf{W}\mathbf{1}_K\mathbf{1}_K^\top.\end{aligned} \tag{22}$$

$\mathbf{w} \in \mathbb{C}^L$ onto the tangent space $\mathcal{T}_{\mathbf{z}}\mathcal{S}^L$ is given by

$$\begin{aligned}\mathbf{P}_{\mathcal{T}_{\mathbf{z}}\mathcal{S}^L}(\mathbf{w}) &= \begin{bmatrix} w_{1r} - \text{Re}\{w_1^* z_1\} z_{1r} + j(w_{1i} - \text{Re}\{w_1^* z_1\} z_{1i}) \\ \vdots \\ w_{Lr} - \text{Re}\{w_L^* z_L\} z_{Lr} + j(w_{Li} - \text{Re}\{w_L^* z_L\} z_{Li}) \end{bmatrix} \\ &= \begin{bmatrix} w_1 - \text{Re}\{w_1^* z_1\} z_1 \\ \vdots \\ w_L - \text{Re}\{w_N^* z_L\} z_L \end{bmatrix} = \mathbf{w} - \text{Re}\{\mathbf{w}^* \odot \mathbf{z}\} \odot \mathbf{z}. \end{aligned} \tag{27}$$

Therefore, the Riemannian gradient of the objective function in (15a) is computed by the projection of the Euclidean gradient computed in (21) onto the tangent space which is given by

$$\nabla_{\mathcal{S}^L} f_1\left(\Gamma_{(i)}\right) = \text{Proj}_{\mathcal{T}_{\mathbf{\Gamma}_{(i)}}\mathcal{S}^L}\left(\nabla f_1\left(\mathbf{\Gamma}_{(i)}\right)\right) \tag{28}$$

$$= \nabla f\left(\mathbf{\Gamma}_{(i)}\right) - \text{Re}\left\{\nabla f_1\left(\mathbf{\Gamma}_{(i)}\right)^* \odot \mathbf{\Gamma}_{(i)}\right\} \odot \mathbf{\Gamma}_{(i)}. \tag{29}$$

After obtaining the Riemannian gradient, the current solution on the CCM is updated iteratively using the following expression

$$\mathbf{\Gamma}_{(k+1)} = \mathbf{\Gamma}_{(k)} + \beta_k \boldsymbol{\eta}_{(k)}, \tag{30}$$

where $\mathbf{\Gamma} = [\omega_1, \omega_2, \cdots, \omega_N]$, $\beta_k \in \mathbb{R}$ and $\boldsymbol{\eta}_{(k)} \in \mathbb{C}^N$ are the step-size and the search direction, respectively. The most common search direction is given by the negative gradient of the objective function represented by the steepest ascent direction. Then, the update formula in (30) is obtained on the tangent space along the direction of the projection with the defined step-size by $\bar{\mathbf{\Gamma}}_{(k)} = \mathbf{\Gamma}_{(k)} - \beta \mathbf{P}_{\mathcal{T}_{\mathbf{\Gamma}_{(k)}}\mathcal{M}}(\nabla_{\mathbf{\Gamma}} f_1(\mathbf{\Gamma}_{(k)}))$. The updated value does not lie on the manifold surface, and thus we need to map it back to the manifold via the retraction operator as follows $\mathbf{\Gamma}_{(k+1)} = \mathbf{R}(\bar{\mathbf{\Gamma}}_{(k)})$.

The derivation for retraction for the CCM is an extension for the (real) unit circle manifold, i.e., $\mathcal{C}^1$. The retraction operator in $\mathcal{S}^L$ is

$$\begin{aligned}\mathbf{R}(\mathbf{w}) &= \begin{bmatrix} \frac{w_{1r}}{\sqrt{w_{1r}^2 + w_{1i}^2}} + j\frac{w_{1i}}{\sqrt{w_{1r}^2 + w_{1i}^2}} \\ \vdots \\ \frac{w_{Lr}}{\sqrt{w_{Lr}^2 + w_{Li}^2}} + j\frac{w_{Li}}{\sqrt{w_{Lr}^2 + w_{Li}^2}} \end{bmatrix} \\ &= \begin{bmatrix} \frac{w_1}{|w_1|} \\ \vdots \\ \frac{w_L}{|w_L|} \end{bmatrix} = \mathbf{w} \odot \frac{1}{|\mathbf{w}|}. \end{aligned} \tag{31}$$

Consequently, the current solution point $\bar{\mathbf{\Gamma}}_{k+1}$ is updated using the retraction mapping in (31), as given by

$$\bar{\mathbf{\Gamma}}_{(k+1)} = \mathbf{\Gamma}_{(k+1)} \odot \frac{1}{|\mathbf{\Gamma}_{(k+1)}|}. \tag{32}$$

The solution for (P5.1) over the CCM is given by the following steps and summarized in Algorithm 1

Algorithm 1 Complex Circle Manifold Based Scheme for RIS Phase Shift Design

Input: $\mathbf{\Gamma}_{(0)} \in \mathcal{M} = \mathcal{S}^N$, β step-size, and stopping criteria threshold ϵ.

Output: A solution $\mathbf{\Gamma}^*$ for (P5.1) over $\mathcal{S}^N$.

(1) Set $k = 0$.
(2) Evaluate the intrinsic (Riemannian) gradient and the decent direction $\boldsymbol{\eta}_{(k)}$.
(3) Project the search dirction $\boldsymbol{\eta}_{(k)}$ onto the tangent space using (27) by $\mathbf{P}_{\mathcal{T}_{\mathbf{\Gamma}_{(k)}}\mathcal{S}^L}\left(\boldsymbol{\eta}_{(k)}\right) = \boldsymbol{\eta}_{(k)} - \text{Re}\{\boldsymbol{\eta}_{(k)}{}^* \odot \mathbf{\Gamma}_{(k)}\} \odot \mathbf{\Gamma}_{(}k)$.
(4) Update $\mathbf{\Gamma_k}$ on the tangent space using $\bar{\mathbf{\Gamma}}_{(k)} = \mathbf{\Gamma}_{(k)} + \beta \mathbf{P}_{\mathcal{T}_{\mathbf{\Gamma}_{(k)}}\mathcal{S}^L}\left(\boldsymbol{\eta}_{(k)}\right)$.
(5) Compute $\mathbf{\Gamma}_{k+1}$ using retraction in (31) as $\mathbf{\Gamma}_{(k+1)} = \mathbf{R}\left(\bar{\mathbf{\Gamma}}_{(k)}\right)$.
(6) Stop if $|\bar{f}_1(\mathbf{\Gamma}_{(k+1)}) - \bar{f}_1(\mathbf{\Gamma}_{(k)})| < \epsilon$.
(7) Set $k = k + 1$.
(8) GOTO step (1).

B. Phase 2: OMO-Based Transmit Beamforming Design

We reformulate the constraint (9d) in (16a) as an oblique manifold (*OM*), $\mathcal{OB}$. The oblique manifold $\mathcal{OB}(n_1, n_2)$ defines the set of all $n_1 \times n_2$ matrices with columns of unity norm [53]. In other words, the complex $\mathcal{OB}(n_1, n_2)$ denotes the embedded sub-manifold of the $n_1 \times n_2$ complex matrices which all have columns with a unit Euclidean norm [54], where

$$\mathcal{OB}(n_1, n_2) = \left\{\mathbf{B} \in \mathbb{C}^{n_1 \times n_2} : \mathbf{I}_{n_1} \circ \left(\mathbf{W}\mathbf{W}^H\right) = \mathbf{I}_{n_1}\right\}. \tag{33}$$

The dimension of $\mathcal{OB}(n_1, n_2)$ is $\dim(\mathcal{OB}) = n1(n2 - 1)$. Therefore, the beamforming matrix $\mathbf{W} = [\mathbf{w_1}, \mathbf{w}_2, \cdots, \mathbf{w}_K] \in \mathbb{C}^{M \times K}$ with $||\mathbf{w}_i||^2 = 1$ $\forall i = 1, \cdots, K$ defines a complex oblique manifold $\mathcal{W}$ such that

$$\mathcal{W} = \left\{\mathbf{W} \in \mathbb{C}^{M \times K} : \mathbf{I}_M \circ \left(\mathbf{W}\mathbf{W}^H\right) = \mathbf{I}_M\right\}. \tag{34}$$

It can be shown that (16a) can be written as the following unconstrained problem

$$\underset{\mathbf{W} \in \mathcal{W}}{\text{maximize}}\ f_2\left(\mathbf{W}\right). \tag{35a}$$

To compute the Riemannian gradient of the objective function in (35a) we need to define both the tangent and normal spaces on the oblique manifold $\mathcal{W}$ at a point. Let $\mathcal{T}_{\mathbf{W}}\mathcal{W}$ and $\mathcal{N}_{\mathbf{W}}\mathcal{W}$ denote the tangent and normal spaces to $\mathcal{W}$ at the point $\mathbf{W}$ and given by, respectively,

$$\mathcal{T}_{\mathbf{W}}\mathcal{W} = \left\{\mathbf{W}_{\|} \in \mathbb{C}^{M \times K} : \mathbf{I}_M \circ \Re\left\{\mathbf{W}\mathbf{W}_{\|}^H\right\} = \mathbf{O}_M\right\}, \tag{36}$$

and

$$\mathcal{N}_{\mathbf{W}}\mathcal{W} = \left\{\mathbf{W}_{\perp}\mathbf{W} : \mathbf{W}_{\perp} \in \mathbb{C}^{M \times M}\text{diagonal}\right\}, \tag{37}$$

where $\mathbf{W}_{\perp} = \mathbf{I}_M \circ \Re\left\{\mathbf{W}(\nabla_{\mathcal{M}}\mathcal{L}_{1b}\left(\mathbf{W}\right))^H\right\}\mathbf{W}$.

As a result, we have the following proposition.

Proposition 2: The Riemannian gradient of $\mathcal{L}_{1b}(\mathbf{W})$ at point $\mathbf{W}$ is obtained by projecting the Euclidean gradient on the tangent space $\mathcal{T}_W\mathcal{W}$ and can be expressed as

$$\nabla_{\mathbf{W}}\mathcal{L}_{1b}(\mathbf{W}) - \mathbf{W}_{\perp}\mathbf{W} \tag{38}$$

where $\mathbf{W}_{\perp}\mathbf{W} \in \mathcal{N}_{\mathbf{W}}\mathcal{W}$. Equivalently,

$$\nabla_{\mathcal{W}}\mathcal{L}_{1b}(\mathbf{W}) = \nabla\mathcal{L}_{1b}(\mathbf{W}) - \left(\mathbf{I}_M \circ \Re\left\{\mathbf{W}(\nabla\mathcal{L}_{1b}(\mathbf{W}))^H\right\}\right)\mathbf{W}. \tag{39}$$

Proof: The proof is provided in Appendix A. □

As mentioned before, a line search on a manifolds can be seen as an extension to that on a Euclidean space. Let $\mathbf{W}_{(t)}$ be the beamforming matrix at the t^{th} iteration, the update formula to maximize the objective function in (35a) is given by

$$\mathbf{W}_{(t+1)} = \mathbf{P}_{\mathcal{W}}\big(\mathbf{W}_{(t)} + \alpha_{(t)}\mathbf{W}_{\perp(t)}\big), \tag{40}$$

where $\mathbf{P}_{\mathcal{W}}(\cdot)$ is the projection onto the oblique manifold, and $\alpha^{(t)}$ is the search step-length, assumed to be the Armijo step-length. At first, the step-size α_0 is set to be 1 along with ξ_0 =1. For $t \geq 1$, the step-size is successively reduced by a certain factor, as in the backtracking line-search [63]. The step-size updating process satisfies

$$\mathcal{L}_{1b}\left(\mathbf{W}^{(t+1)}\right) - \mathcal{L}_{1b}\left(\mathbf{W}^{(t)}\right) \leq -\frac{1}{2}\alpha^{(t)}\|\text{vec}(\text{grad}f_2(\mathbf{W}_t)\|^2. \tag{41}$$

In fact, the projection of a point $\mathbf{P}$ onto a set $\mathcal{W}$ minimizes the distance of $\mathbf{P}$ to $\mathcal{W}$. The projection of $\mathbf{W}$ onto a manifold $\mathcal{W}$ is given by

$$\mathbf{P}_{\mathcal{W}}(\mathbf{W}) = \left(\mathbf{I}_M \circ \left(\mathbf{W}\mathbf{W}^H\right)\right)^{-1/2}\mathbf{W}. \tag{42}$$

Performing line search algorithms on Riemannian manifolds, including the oblique manifold $\mathcal{W}$, requires a retraction definition. In order to guarantee that the generating $\mathbf{W}^{(t)}$'s stay on the manifold, the retraction maps between points on the manifold and its tangent space [49]. For simplicity, we adopt the projection concept in this paper, i.e.,

$$\langle \mathbf{W}_1, \mathbf{W}_2\rangle := \text{trace}(\mathbf{W}_1^{\text{T}}\mathbf{W}_2), \tag{43}$$

It is known that coupling the Armijo's step-size with the SD algorithm always converges to a local minimum [51].

The termination criteria for the SD-OMO algorithm is defined when the gradient at iteration $t+1$ satisfies [53]

$$\|\text{vec}(\text{grad}f_2(\mathbf{W}_{t+1}))\|_\infty < \epsilon(1 + \|\text{vec}(\text{grad}f_2(\mathbf{W}_0))\|_\infty), \tag{44}$$

where ϵ is an accuracy parameter that we set to 10^{-7}.

C. Complexity Analysis

The computation of the gradients in (21) and (22), and their projections onto the tangent spaces of $\mathcal{M}$ and $\mathcal{W}$, respectively, determine the complexity of the overall algorithm. We present the analytic complexity in terms of floating point operations (flops) which include any multiplication, division, addition, or subtraction operation of two floating point numbers. The complexity of each iteration in the proposed approach is as follows:

Algorithm 2 Line Search Approach for Transmit Beamforming $\mathbf{W}$

Input: $\mathbf{W}_0 = \mathbf{I}_{M\times K}$, $\alpha^{(k)}$ step-size, and stopping criteria threshold ϵ_0.

Output: Optimal $\mathbf{W}^*$.

for k = 0 **do**
  Compute the Euclidean gradient in (22).
  Evaluate the intrinsic (Riemannian) gradient using (39).
  Evaluate $\mathbf{W}_{\perp} = \mathbf{I}_M \circ \Re\left\{\mathbf{W}(\nabla_{\mathcal{M}}\mathcal{L}_{1b}(\mathbf{W}))^H\right\}\mathbf{W}$.
  Compute the Armijo step-size.
  Evaluate $\left(\mathbf{W}^{(t)} + \alpha^{(t)}\mathbf{W}_{\perp}{}^{(t)}\right)$.
  Evaluate the Projection using (40).
  if

$$\|\text{vec}(\text{grad}f_2(\mathbf{W}_{t+1}))\|_\infty < \epsilon(1+\|\text{vec}(\text{grad}f_2(\mathbf{W}_0))\|_\infty)$$

  then Stop
  end if
end for

- The gradients in (21) and (22) are $\mathcal{O}(K^4(ML)^2 + N^4)$ and $\mathcal{O}(K^2M + N^2MK + N^2KL_R)$.
- The projection operations in (39) and (42) are $\mathcal{O}(N)$ and $\mathcal{O}(M^3/3 + M^2K + M)$.
- Update formulas are $2N+1$ and $MK(2M-1)$ multiplications and $\mathcal{O}(M^3/2)$ for matrix inversion.

V. Numerical Results

This section presents the results of Monte Carlo simulations to validate the effectiveness of the proposed RIS-aided MIMO radar and MU-MIMO communication spectrum sharing system. We average the results over $2,000$ independent realizations. All channel matrices are generated as independent and identically distributed matrices. For simplicity, we assume that the radar transmitter and the communication BS are both equipped with uniform linear arrays with an inter-element spacing of $\frac{\lambda}{2}$. However, we assume a uniform planar array configuration at the RIS, where the size of the RIS $N = N_h \times N_v$ and we set $N_h = 10$. The array responses for the transmit and receive radar array are equal $\mathbf{a}_T = \mathbf{a}_R = \mathbf{a}$. The average noise power is set to -30 dB, the BS power budget is $P = 40\ dBm$, and the radar SNR is defined as $\text{SNR}_{\text{R}} = \text{P}_{\text{R}}|\alpha|^2\text{L}/\sigma_{\text{R}}^2$ [35], where L is the length of the communication frame.

Next, we present the following benchmark approaches with which to compare our proposed approach.

1) **Random Phase Shifts:** In this benchmark scheme, the phase shift matrix is set randomly, while, the beamforming matrix is computed by solving (35a).
2) **Zero-forcing (ZF) Beamforming:** ZF-beamforming is defined as

$$\mathbf{W}_{\text{ZF}} = \frac{1}{f_{\text{ZF}}} \cdot \mathbf{H}^{\text{H}}\left(\mathbf{H}\mathbf{H}^{\text{H}}\right)^{-1}, \tag{45}$$

where f_{ZF} refers to the noise amplification factor, i.e., normalization factor, which guarantees the transmit

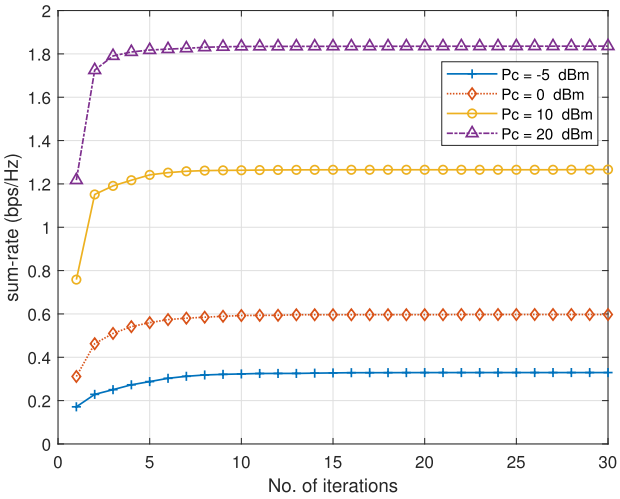

Fig. 2. Sum-rate for the communication system versus number of iterations for different BS power budgets.

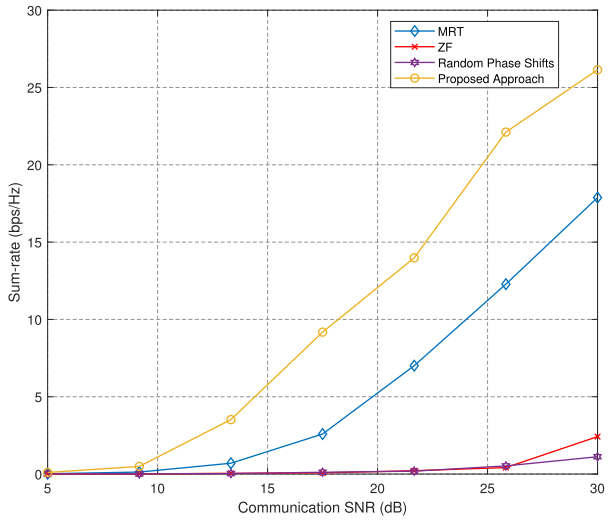

Fig. 3. The sum-rate against communication system SNR comparison with benchmark schemes.

power is not increased after applying the beamforming. In our case, the normalization factor is given by $f_{\mathrm{ZF}} = \sqrt{\mathrm{tr}\left\{(\mathbf{H}\mathbf{H}^{\mathrm{H}})^{-1}\right\}}$. The phase shift matrix is updated by solving (23a). We alternate to find the optimal phase shift matrix and the beamforming matrix.

3) **Maximum Ratio Transmission (MRT) Beamforming**: The MRT beamformer is expressed as

$$\mathbf{W}_{\mathrm{MRT}} = \frac{\mathbf{H}}{||\mathbf{H}||_F^2}. \tag{46}$$

As with the ZF approach, the phase shift matrix is updated by solving (23a). We alternate to optimize the phase shift and the beamforming matrices.

Fig. 2 depicts the convergence of the proposed approach with $N = 10$, $M = K = 8$, and $L = 1$ for different BS power budgets. It can be observed that the sum-rate monotonically increases with the number of iterations and converges in about 10 iterations for different BS power budgets. It is also seen that the sum-rate increases as the BS power budget P_C increases as well. Specifically, the proposed approach takes less than

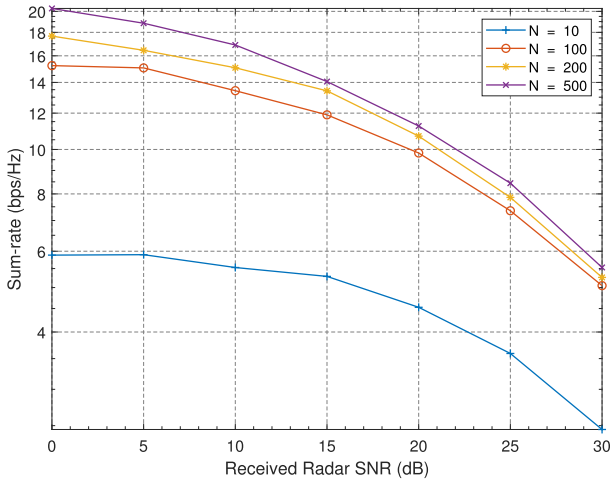

Fig. 4. Communication system sum-rate against the number of the RIS reflecting elements of with different received radar SNR.

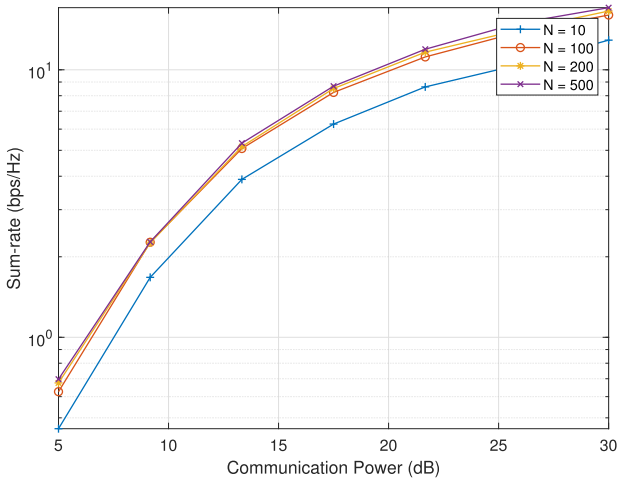

Fig. 5. Communication system sum-rate against the number of the reflecting elements of the RIS with different communication system SNR.

5 iterations when $P_C = 20\mathrm{dBm}$ and $30\mathrm{dBm}$, respectively, while 10 iterations are required for $P_C \leq 0\mathrm{dBm}$. Consequently, Fig. 2 demonstrates the effectiveness of the proposed approach in mitigating the mutual interference between the radar and communication systems and improving the sum-rate for the communication system. As a result, the proposed algorithms are guaranteed to converge. In Fig. 3, we compare the sum-rate obtained by the proposed approach with the benchmark schemes. We set $N = 120$, $M = 12$, $K = 10$, and the receive radar SNR = 0 dB. It can be observed that both ZF and the random RIS phase shift approaches fail to find the optimal BS beamformer and RIS phase shifts. The performance of ZF highly depends on the number of users and the SNR regime. Specifically, the ZF reaches its optimal performance when the ComUTs channels are orthogonal. In addition, the ZF does not consider the noise and the radar interference thus it performs poorly. On the other hand, the MRT beamforming method aims to maximize the received power for ComUTs without considering the interference. However, the proposed approach outperforms MRT.

In Figs. 4-5, we show the impact of the number of RIS reflecting elements N on the performance of the proposed

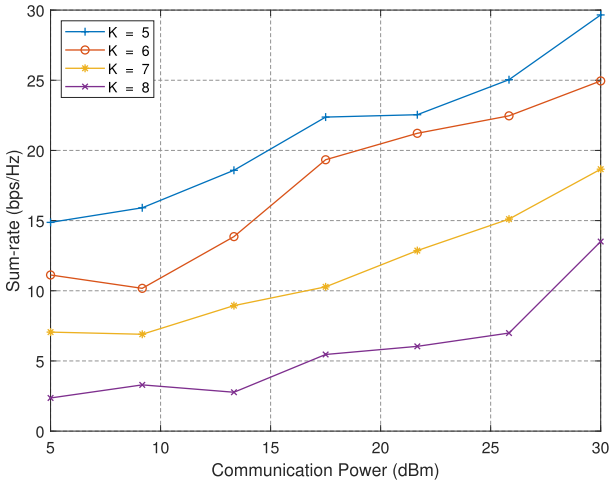

Fig. 6. The sum-rate against communication system SNR for different K.

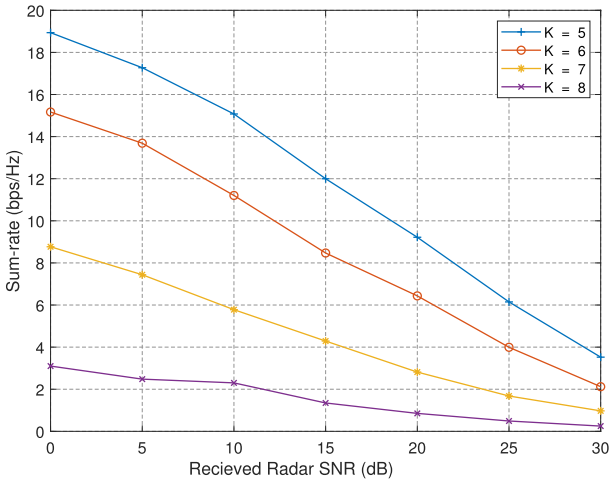

Fig. 7. The sum-rate against received radar SNR for different K, when $N = 100$.

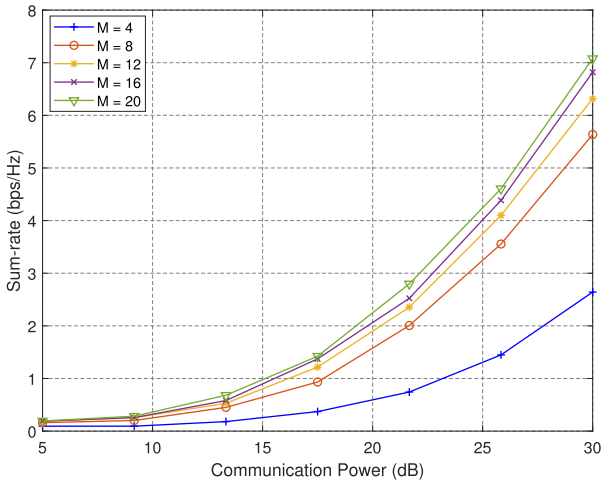

Fig. 8. The ComUTs sum-rate against received radar SNR for different M, when $N = 100$.

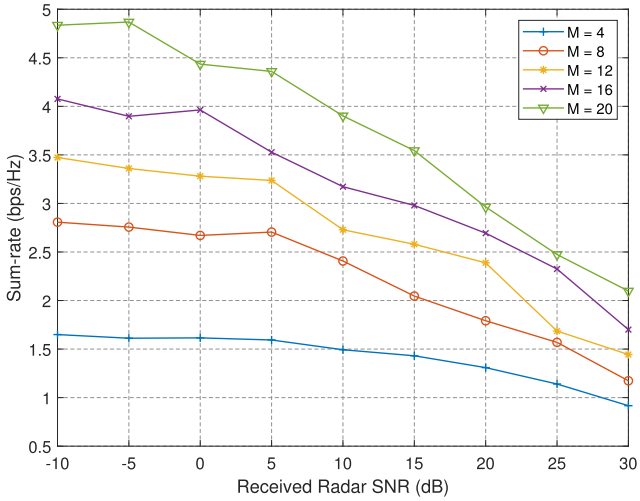

Fig. 9. The sum-rate against communication system SNR for different M.

approach. Fig. 4 compares the sum-rate for the communication systems with respect to (w.r.t.) the received radar SNR for different N. Fig. 5 shows the sum-rate w.r.t. the communication system SNR for varying N. It can be seen that the sum-rate for the ComUTs increases with N despite the existence of radar operation, since a larger RIS is able to provide a higher passive beamforming gain and a better capability to reduce the MUI and the interference power from the BS.

In Fig. 6, we compare the sum-rate against communication system SNR for different numbers of ComUTs. In Fig. 6, we set $N = 100$, P_r = 10 dB, and $\hat{p}_0$ = -30 dBm. Unsurprisingly, the sum-rate decreases as the number of ComUTs K increases, since the MUI term grows. Furthermore, it can be observed that the communication system performance in the proposed framework is enhanced by increasing the SNR for the communication system. On average, the sum-rate is increased by 170% and 60% when the number of ComUTs decreases from $K = 8$ to $K = 5$ and the communication system SNR increases from 5 dB to 30 dB, respectively.

Fig. 7 depicts the sum-rate for the communication system, where different received radar SNR and numbers of ComUTs are considered. We assume $N = 100$, $\hat{p}_0$ = -30 dBm $M = 20$, $K = 4$, and a communication system SNR of 5 dB. As the results show, the sum-rate decreases as the radar SNR and number of ComUTs increase. The received radar SNR increases by either increasing the radar transmit power P_r, or reducing the interference. As a consequence of growing P_r, the communication SINR decreases as does the sum-rate. Moreover, the proposed approach guarantees the operation of the radar system by reducing the interference through optimization of the RIS phase shifts matrix and the BS beamformer. Subsequently, the SINR for the ComUTs decreases with the radar SNR.

Figs. 8-9 depict the effect of the number of BS antennas M on the communication system performance. As the results illustrate in Figs. 8-9, the sum-rate of the communication system increases with M since the array gain provided by the BS increases. A sum-rate enhancement of 180% can be achieved for the ComUTs by increasing M from 4 to 8. Moreover, the increase in communication system SNR leads to enhanced ComUTs sum-rate, as shown in Fig. 8. On the other hand, ComUTs sum-rate decreases with an increase of the received radar SNR as shown in Fig. 9.

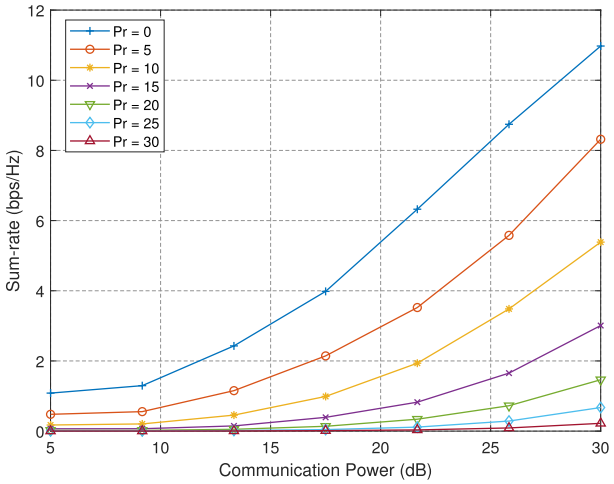

Fig. 10. The ComUTs sum-rate against communication system SNR for different radar transmit power budget P_R.

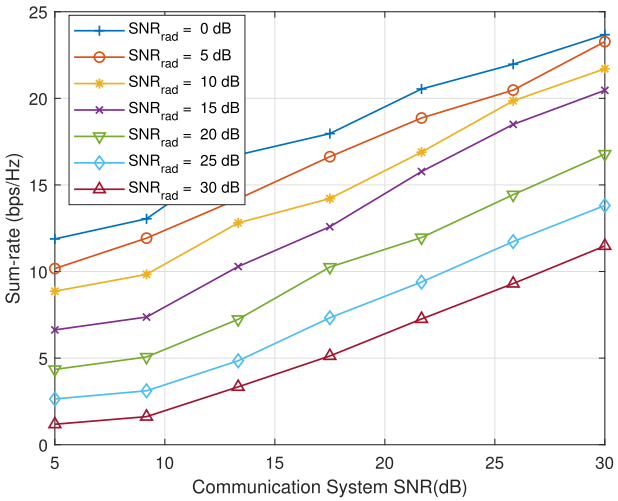

Fig. 11. The ComUTs sum-rate against communication system SNR for different received radar SNR.

Fig. 10 compares the ComUTs sum-rate w.r.t. the communication system SNR for varying radar transmit power budgets. It can be seen that the proposed scheme provides a monotonic increase in the communication system sum-rate as the communication system SNR increases. However, the ComUTs sum-rate decreases with an increase in the radar transmit power budget as the interfering power from the radar transmitter increases. Fig. 11 illustrates the performance of the proposed scheme versus the communication SNRs for different received radar SNR. It is obvious that there is a trade-off between the communication and radar systems performance. The sum-rate of the ComUTs provided by the proposed approach increases with increased of the communication system SNR and decreased received radar SNR.

Fig. 12 captures the RIS capability to eliminate the mutual interference, i.e., $P_{int}/\hat{p_0}$, between the radar and communication systems. We study the mutual interference versus on the radar system versus the communication transmit power. We assume that the $\hat{p_0} = 0$ dBm $M = 20$, $K = 4$. It can be seen that the RIS is capable of maintaining the interfering power within threshold value. In addition, we can see that

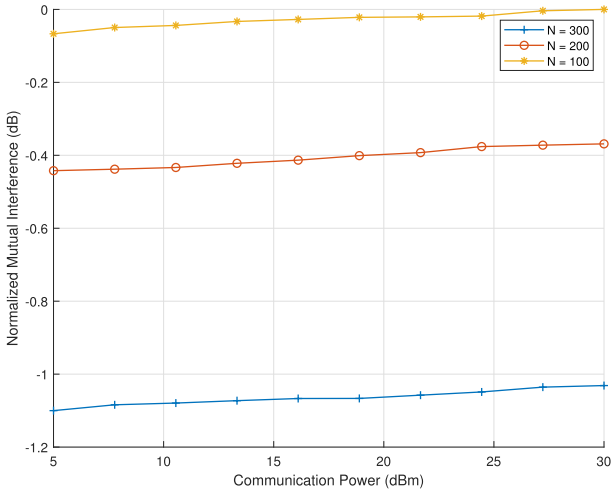

Fig. 12. The normalized mutual interference power against communication system SNR for different RIS elements.

the mutual interference level decreases with the increase of the number of the RIS elements. Since the RIS ability to beamform and boost the received SNR enhances with the increase of reflecting elements number.

VI. Conclusion

In this paper, we have investigated a new approach to improve the performance of a MU-MIMO radar and communication coexistence system by exploiting the deployment of an RIS. We have formulated the sum-rate maximization problem for the communication system by optimizing the transmit beamforming vectors and the RIS phase shifts to maximize the communication system performance subject to constraints on the interference from the communication system to the radar system and the transmit power budget. We have proposed a search algorithm based on manifold optimization, and then implemented using alternating optimization. The original problem was transformed into a simpler form using the FP method, and a line search approach was conducted over the manifold instead of using algorithms on the Euclidean space. Moreover, we divided the original problem into two sub-problems over two different manifolds. The simulation results demonstrated the efficiency and effectiveness of the proposed approach. Our approach was able to maximize the communication system sum-rate while maintaining the communication system interference below a certain threshold. Numerical results showed that there is a trade-off between communication and radar system performance and that we can enhance the performance of both systems by increasing the number of the RIS reflecting elements, since a larger RIS is able to provide a higher passive beamforming gain and is more capable of reducing the mutual interference between the radar and communication systems.

Appendix A

The tangent space to the embedded sub-manifold $\mathcal{W}$ is given in (36). The oblique manifold is a regular sub-manifold such that there is a unique differentiable structure on the

manifold. That allows expressing the canonical inner product using sub-manifold theory as follows

$$\langle \mathbf{A}, \mathbf{B} \rangle \triangleq \Re \left\{ \mathrm{tr} \left(\mathbf{A}^H \mathbf{B} \right) \right\}, \tag{47}$$

where $\mathbf{A}$, $\mathbf{B} \in \mathbb{C}^{M \times K}$. Equivalently, (47) treats $\mathbb{C}^{M \times K}$ as $\mathbb{R}^{2M \times 2\ K}$. The normal space defined in (37) represents the orthogonal complement of the tangent space in (36) with respect to the metric of the ambient Euclidean space $\mathcal{A}$, i.e., and it depends on the embedding in the Euclidean space. According to (47), we have

$$\left\langle \mathbf{W}_{\parallel}, \mathbf{W}_{\perp} \right\rangle_{\mathcal{A}} = \Re \left\{ \mathrm{tr} \left({\mathbf{W}_{\parallel}}^H \mathbf{W}_{\perp} \right) \right\} = 0, \tag{48}$$

where $\mathbf{W}_{\parallel} \in T_{\mathbf{W}}\mathcal{W}$ and $\mathbf{W}_{\perp} \in N_{\mathbf{W}}\mathcal{W}$. According (36) and (48), the normal space to $\mathcal{W}$ at a point $\mathbf{W}_1$ is $N_{\mathbf{W}_1}\mathcal{M} = \left\{ \mathbf{D}\mathbf{W}_1 : \mathbf{D} \in \mathbb{C}^{M \times M} \mathrm{diagonal} \right\}$. Using $\Re \left\{ \mathrm{tr} \left(\left(\nabla \mathcal{L}_{1b} \left(\mathbf{W}_1 \right) - \mathbf{D}\mathbf{W}_1 \right)^H \mathbf{D}\mathbf{W}_1 \right) \right\} = 0$ yields $\mathbf{W}_1 = \mathbf{I}_M \circ \Re \left\{ \mathbf{W}_1 (\nabla \mathcal{L}_{1b} \left(\boldsymbol{W}_1 \right))^H \right\} \mathbf{W}_1$. Therefore, let $\nabla_{\mathcal{M}} \mathcal{L}_{1b} \left(\mathbf{W} \right)$ denote the Riemannian gradient of the objective function in (35a) at the point $\mathbf{W}$. The Riemannian gradient is computed by projecting the gradient onto the tangent space $T_{\mathbf{W}}\mathcal{W}$, i.e.

$$\begin{aligned} \nabla_{\mathcal{W}} \mathcal{L}_{1b} \left(\boldsymbol{W} \right) &= \nabla \mathcal{L}_{1b} \left(\mathbf{W} \right) \\ &\quad - \left(\mathbf{I}_M \circ \Re \left\{ \mathbf{W} (\nabla \mathcal{L}_{1b} \left(\boldsymbol{W} \right))^H \right\} \right) \mathbf{W}. \end{aligned} \tag{49}$$

REFERENCES

[1] H. Deng and B. Himed, "Interference mitigation processing for spectrum-sharing between radar and wireless communications systems," *IEEE Trans. Aerosp. Electron. Syst.*, vol. 49, no. 3, pp. 1911–1919, Jul. 2013.

[2] S. Amuru, R. M. Buehrer, R. Tandon, and S. Sodagari, "MIMO radar waveform design to support spectrum sharing," in *Proc. MILCOM IEEE Mil. Commun. Conf.*, Nov. 2013, pp. 1535–1540.

[3] C. Shahriar, A. Abdelhadi, and T. C. Clancy, "Overlapped-MIMO radar waveform design for coexistence with communication systems," in *Proc. IEEE Wireless Commun. Netw. Conf. (WCNC)*, Mar. 2015, pp. 223–228.

[4] A. Khawar, A. Abdelhadi, and C. Clancy, "Target detection performance of spectrum sharing MIMO radars," *IEEE Sensors J.*, vol. 15, no. 9, pp. 4928–4940, Sep. 2015.

[5] J. A. Mahal, A. Khawar, A. Abdelhadi, and T. C. Clancy, "Spectral coexistence of MIMO radar and MIMO cellular system," *IEEE Trans. Aerosp. Electron. Syst.*, vol. 53, no. 2, pp. 655–668, Apr. 2017.

[6] J. Li and P. Stoica, "MIMO radar with colocated antennas," *IEEE Signal Process. Mag.*, vol. 24, no. 5, pp. 106–114, Sep. 2007.

[7] M. I. Skolnik, *Radar Handbook*, 3rd ed. New York, NY, USA: McGraw-Hill, 2008.

[8] B. Li, A. P. Petropulu, and W. Trappe, "Optimum co-design for spectrum sharing between matrix completion based MIMO radars and a MIMO communication system," *IEEE Trans. Signal Process.*, vol. 64, no. 17, pp. 4562–4575, Sep. 2016.

[9] Q. Nadeem, A. Kammoun, M. Debbah, and M. Alouini, "A generalized spatial correlation model for 3D MIMO channels based on the Fourier coefficients of power spectrums," *IEEE Trans. Signal Process.*, vol. 63, no. 14, pp. 3671–3686, Jul. 2015.

[10] X. Yu, J. Shen, J. Zhang, and K. B. Letaief, "Alternating minimization algorithms for hybrid precoding in millimeter wave MIMO systems," *IEEE J. Sel. Topics Signal Process.*, vol. 10, no. 3, pp. 485–500, Apr. 2016.

[11] L. Zheng, M. Lops, Y. C. Eldar, and X. Wang, "Radar and communication coexistence: An overview: A review of recent methods," *IEEE Signal Process. Mag.*, vol. 36, no. 5, pp. 85–99, Sep. 2019.

[12] M. Rihan and L. Huang, "Optimum co-design of spectrum sharing between MIMO radar and MIMO communication systems: An interference alignment approach," *IEEE Trans. Veh. Technol.*, vol. 67, no. 12, pp. 11667–11680, Dec. 2018.

[13] O. E. Ayach, S. Rajagopal, S. Abu-Surra, Z. Pi, and R. W. Heath, "Spatially sparse precoding in millimeter wave MIMO systems," *IEEE Trans. Wireless Commun.*, vol. 13, no. 3, pp. 1499–1513, Mar. 2014.

[14] C. Balanis, *Antenna Theory*, Hoboken, NJ, USA: Wiley, 1997.

[15] T. David and P. Viswanath, *Fundamentals of Wireless Communication*. Cambridge, U.K.: Cambridge Univ. Press, 2005.

[16] B. Li and A. Petropulu, "Radar precoding for spectrum sharing between matrix completion based MIMO radars and a MIMO communication SYSTEM," in *Proc. IEEE Global Conf. Signal Inf. Process. (GlobalSIP)*, Dec. 2015, pp. 737–741.

[17] B. Li, H. Kumar, and A. P. Petropulu, "A joint design approach for spectrum sharing between radar and communication systems," in *Proc. IEEE Int. Conf. Acoust., Speech Signal Process. (ICASSP)*, Mar. 2016, pp. 3306–3310.

[18] B. Li and A. Petropulu, "MIMO radar and communication spectrum sharing with clutter mitigation," in *Proc. IEEE Radar Conf. (RadarConf)*, May 2016, pp. 1–6.

[19] B. Li and A. Petropulu, "Spectrum sharing between matrix completion based MIMO radars and a MIMO communication system," in *Proc. IEEE Int. Conf. Acoust., Speech Signal Process. (ICASSP)*, Apr. 2015, pp. 2444–2448.

[20] J. Kota, G. Jacyna, and A. Papandreou-Suppappola, "Nonstationary signal design for coexisting radar and communications systems," in *Proc. 50th Asilomar Conf. Signals, Syst. Comput.*, Pacific Grove, CA, USA, Nov. 2016, pp. 549–553.

[21] R. A. Romero and K. D. Shepherd, "Friendly spectrally shaped radar waveform with legacy communication systems for shared access and spectrum management," *IEEE Access*, vol. 3, pp. 1541–1554, 2015.

[22] J. T. Johnson, C. J. Baker, H. Wang, L. Ye, and C. Zhang, "Assessing the potential for spectrum sharing between communications and radar systems in the L-band portion of the RF spectrum allocated to radar," in *Proc. Int. Conf. Electromagn. Adv. Appl. (ICEAA)*, Aug. 2014, pp. 331–334.

[23] A. Babaei, W. H. Tranter, and T. Bose, "A nullspace-based precoder with subspace expansion for radar/communications coexistence," in *Proc. IEEE Global Commun. Conf. (GLOBECOM)*, Dec. 2013, pp. 3487–3492.

[24] B. Kang, O. Aldayel, V. Monga, and M. Rangaswamy, "Spatio-spectral radar beampattern design for coexistence with wireless communication systems," *IEEE Trans. Aerosp. Electron. Syst.*, vol. 55, no. 2, pp. 644–657, Apr. 2019.

[25] C. Kotchasarn, "Power allocation for multi-user downlink MIMO transmissions," in *Proc. IEEE Int. Conf. Innov. Res. Develop. (ICIRD)*, May 2018, pp. 1–5.

[26] D. R. Fuhrmann and G. S. Antonio, "Transmit beamforming for MIMO radar systems using signal cross-correlation," *IEEE Trans. Aerosp. Electron. Syst.*, vol. 44, no. 1, pp. 171–186, Jan. 2008.

[27] P. Stoica, J. Li, and X. Zhu, "Waveform synthesis for diversity-based transmit beampattern design," *IEEE Trans. Signal Process.*, vol. 56, no. 6, pp. 2593–2598, Jun. 2008.

[28] S. Ahmed, J. S. Thompson, Y. R. Petillot, and B. Mulgrew, "Unconstrained synthesis of covariance matrix for MIMO radar transmit beampattern," *IEEE Trans. Signal Process.*, vol. 59, no. 8, pp. 3837–3849, Aug. 2011.

[29] A. Khabbazibasmenj, S. A. Vorobyov, A. Hassanien, and M. W. Morency, "Transmit beamspace design for direction finding in colocated MIMO radarwith arbitrary receive array and even number of waveforms," in *Proc. Conf. Rec. 46th Asilomar Conf. Signals, Syst. Comput. (ASILOMAR)*, Nov. 2012, pp. 1307–1311.

[30] Y.-H. Tang, X.-F. Ma, W.-X. Sheng, and Y.-B. Han, "A new transmit beamforming algorithm for subarray MIMO radar," in *Proc. IEEE Int. Symp. Phased Array Syst. Technol.*, Oct. 2013, pp. 255–258.

[31] D. R. Fuhrman, J. P. Browning, and M. Rangaswamy, "Adapting a MIMO/phased-array radar transmit beampattern to target location," in *Proc. 2nd Int. Workshop Cognit. Inf. Process.*, Jun. 2010, pp. 354–359.

[32] Y. Li, Y. Zhang, and W. Xie, "Joint transmit-receive subarray synthesis optimization for hybrid MIMO phased-array radar," in *Proc. 10th Int. Congr. Image Signal Process., Biomed. Eng. Informat. (CISP-BMEI)*, Oct. 2017, pp. 1–6.

[33] Z. Chen, H. Li, G. Cui, and M. Rangaswamy, "Adaptive transmit and receive beamforming for interference mitigation," *IEEE Signal Process. Lett.*, vol. 21, no. 2, pp. 235–239, Feb. 2014.

[34] W. Roberts, J. Li, P. Stoica, and X. Zhu, "MIMO radar receiver design," in *Proc. IEEE Radar Conf.*, May 2008, pp. 1–6.

[35] I. Bekkerman and J. Tabrikian, "Target detection and localization using MIMO radars and sonars," *IEEE Trans. Signal Process.*, vol. 54, no. 10, pp. 3873–3883, Oct. 2006.

[36] E. Grossi, M. Lops, and L. Venturino, "Joint design of surveillance radar and MIMO communication in cluttered environments," *IEEE Trans. Signal Process.*, vol. 68, pp. 1544–1557, 2020.

[37] F. Liu, C. Masouros, A. Li, T. Ratnarajah, and J. Zhou, "MIMO radar and cellular coexistence: A power-efficient approach enabled by interference exploitation," *IEEE Trans. Signal Process.*, vol. 66, no. 14, pp. 3681–3695, Jul. 2018.

[38] J. Chen, "Manifold optimization approach for data detection in massive multiuser MIMO systems," *IEEE Trans. Veh. Technol.*, vol. 67, no. 4, pp. 3652–3657, Apr. 2018.

[39] K. Alhujaili, V. Monga, and M. Rangaswamy, "Transmit MIMO radar beampattern design via optimization on the complex circle manifold," *IEEE Trans. Signal Process.*, vol. 67, no. 13, pp. 3561–3575, Jul. 2019.

[40] Y. Cui, V. Koivunen, and X. Jing, "Interference alignment based precoder-decoder design for radar-communication co-existence," in *Proc. 51st Asilomar Conf. Signals, Syst., Comput.*, Oct. 2017, pp. 1290–1295.

[41] S. Fang, G. Chen, P. Xu, J. Tang, and J. A. Chambers, "SINR maximization for RIS-assisted secure dual-function radar communication systems," in *Proc. IEEE Global Commun. Conf. (GLOBECOM)*, Dec. 2021, pp. 1–6.

[42] X. Song, D. Zhao, H. Hua, T. X. Han, X. Yang, and J. Xu, "Joint transmit and reflective beamforming for IRS-assisted integrated sensing and communication," in *Proc. IEEE Wireless Commun. Netw. Conf. (WCNC)*, Apr. 2022, pp. 189–194.

[43] Z. Esmaeilbeig, K. V. Mishra, and M. Soltanalian, "IRS-aided radar: Enhanced target parameter estimation via intelligent reflecting surfaces," in *Proc. IEEE 12th Sensor Array Multichannel Signal Process. Workshop (SAM)*, Jun. 2022, pp. 286–290.

[44] X. Wang, Z. Fei, J. Huang, and H. Yu, "Joint waveform and discrete phase shift design for RIS-assisted integrated sensing and communication system under Cramer–Rao bound constraint," *IEEE Trans. Veh. Technol.*, vol. 71, no. 1, pp. 1004–1009, Jan. 2022.

[45] Z. Jiang et al., "Intelligent reflecting surface aided dual-function radar and communication system," *IEEE Syst. J.*, vol. 16, no. 1, pp. 475–486, Mar. 2022.

[46] T. Wei, L. Wu, K. V. Mishra, and M. R. B. Shankar, "Multiple IRS-assisted wideband dual-function radar-communication," in *Proc. 2nd IEEE Int. Symp. Joint Commun. Sens. (JC&S)*, Mar. 2022, pp. 1–5.

[47] M. Un, W. Ma, and P. C. Ching, "Joint transmit beamforming optimization and uplink/downlink user selection in a full-duplex multi-user MIMO system," in *Proc. IEEE Int. Conf. Acoust., Speech Signal Process. (ICASSP)*, Mar. 2017, pp. 3639–3643.

[48] J. Qian, Z. He, N. Huang, and B. Li, "Transmit designs for spectral coexistence of MIMO radar and MIMO communication systems," *IEEE Trans. Circuits Syst. II, Exp. Briefs*, vol. 65, no. 12, pp. 2072–2076, Dec. 2018.

[49] P. Zhou, X. Yuan, S. Yan, and J. Feng, "Faster first-order methods for stochastic non-convex optimization on Riemannian manifolds," *IEEE Trans. Pattern Anal. Mach. Intell.*, vol. 43, no. 2, pp. 459–472, Feb. 2021.

[50] A. Epstein and G. V. Eleftheriades, "Synthesis of passive lossless metasurfaces using auxiliary fields for reflectionless beam splitting and perfect reflection," *Phys. Rev. Lett.*, vol. 117, no. 25, Dec. 2016, Art. no. 256103.

[51] P.-A. Absil, R. Mahony, and R. Sepulchre, *Optimization Algorithms on Matrix Manifolds*, Princeton, NJ, USA: Princeton Univ. Press, 2009.

[52] E. Shtaiwi, H. Zhang, A. Abdelhadi, and Z. Han, "Sum-rate maximization for RIS-assisted radar and communication coexistence system," in *Proc. IEEE Global Commun. Conf. (GLOBECOM)*, Dec. 2021, pp. 1–6.

[53] P.-A. Absil and K. A. Gallivan, "Joint diagonalization on the oblique manifold for independent component analysis," in *Proc. IEEE Int. Conf. Acoust. Speed Signal Process.*, May 2006, p. 5.

[54] H. Kasai, "Fast optimization algorithm on complex oblique manifold for hybrid precoding in millimeter wave MIMO systems," in *Proc. IEEE Global Conf. Signal Inf. Process. (GlobalSIP)*, Nov. 2018, pp. 1266–1270.

[55] K. Shen and W. Yu, "Fractional programming for communication systems—Part II: Uplink scheduling via matching," *IEEE Trans. Signal Process.*, vol. 66, no. 10, pp. 2631–2644, May 2018.

[56] F. Liu, C. Masouros, A. Li, H. Sun, and L. Hanzo, "MU-MIMO communications with MIMO radar: From co-existence to joint transmission," *IEEE Trans. Wireless Commun.*, vol. 17, no. 4, pp. 2755–2770, Apr. 2018.

[57] E. Shtaiwi, H. Zhang, A. Abdelhadi, and Z. Han, "RIS-assisted mmWave channel estimation using convolutional neural networks," in *Proc. IEEE Wireless Commun. Netw. Conf. Workshops (WCNCW)*, Mar. 2021, pp. 1–6.

[58] R. Feng, C. Wang, J. Huang, X. Gao, S. Salous, and H. Haas, "Classification and comparison of massive MIMO propagation channel models," *IEEE Internet Things J.*, vol. 9, no. 23, pp. 23452–23471, Dec. 2022.

[59] C. Chen and O. L. Mangasrian, "Smoothing methods for convex inequalities and linear complementarity problems exact penalty functions for convex constrained optimization," *Math. Program.*, vol. 71, pp. 51–69, Nov. 1995.

[60] J. Nocedal and S. Wright, *Numerical Optimization*. Cham, Switzerland: Springer, 2006.

[61] Z. Lu, Y. Zhang, and X. Li, "Penalty decomposition methods for rank minimization," *Optim. Methods Softw.*, vol. 30, no. 3, pp. 531–558, May 2015.

[62] E. Shtaiwi, H. Zhang, S. Vishwanath, M. Youssef, A. Abdelhadi, and Z. Han, "Channel estimation approach for RIS assisted MIMO systems," *IEEE Trans. Cognit. Commun. Netw.*, vol. 7, no. 2, pp. 452–465, Jun. 2021.

[63] Z. Li, D. Zhao, Z. Lin, and E. Y. Chang, "Determining step sizes in geometric optimization algorithms," in *Proc. IEEE Int. Symp. Inf. Theory (ISIT)*, Jun. 2015, pp. 1217–1221.

[64] B. Li and A. P. Petropulu, "Joint transmit designs for coexistence of MIMO wireless communications and sparse sensing radars in clutter," *IEEE Trans. Aerosp. Electron. Syst.*, vol. 53, no. 6, pp. 2846–2864, Dec. 2017.

Eyad Shtaiwi (Graduate Student Member, IEEE) received the B.S. and M.S. degrees in communication engineering and wireless communication engineering from Yarmouk University, Irbid, Jordan, in 2012 and 2015, respectively. He is currently pursuing the Ph.D. degree with the Department of Electrical and Computer Engineering, University of Houston, Houston, TX, USA. His research interests include advanced areas of wireless communications, including massive and mmWave MIMO systems, signal processing, and wireless channel modeling and estimation.

Hongliang Zhang (Member, IEEE) received the B.S. and Ph.D. degrees from the School of Electrical Engineering and Computer Science, Peking University, in 2014 and 2019, respectively. He is currently an Assistant Professor with the School of Electronics, Peking University. His current research interests include reconfigurable intelligent surfaces, aerial access networks, the Internet of Things, optimization theory, and game theory. He has served as a TPC member and the workshop co-chair for many IEEE conferences. He was a recipient of the 2021 IEEE Comsoc Heinrich Hertz Award for Best Communications Letters and the 2021 IEEE ComSoc Asia-Pacific Outstanding Paper Award. He received the Best Doctoral Thesis Award from the Chinese Institute of Electronics in 2019. He is the winner of the Outstanding Leadership Award as the Publicity Chair for IEEE EUC in 2022. He is an Editor for IEEE TRANSACTIONS ON VEHICULAR TECHNOLOGY, IEEE COMMUNICATIONS LETTERS, *IET Communications*, and *Frontiers in Signal Processing*. He has also served as the Guest Editor for several journals, such as IEEE INTERNET OF THINGS JOURNAL and *Journal of Communications and Networks*. He was an Exemplary Reviewer of IEEE TRANSACTIONS ON COMMUNICATIONS in 2020.

Ahmed Abdelhadi (Senior Member, IEEE) received the Ph.D. degree in electrical and computer engineering from The University of Texas at Austin in 2011. He was a member with the Wireless Networking and Communications Group (WNCG) and the Laboratory of Informatics, Networks, and Communications Group during the Ph.D. degree. In 2012, he joined the Bradley Department of Electrical and Computer Engineering and the Hume Center for National Security and Technology, Virginia Tech, where he was a Faculty Member of Wireless@VT Research Group. He is currently an Assistant Professor with the University of Houston (UH) and the Director of the Communications, Artificial Intelligence, Systems, and Security (CAISS) Laboratory, UH. Before joining UH, he was a Research Assistant Professor with Virginia Tech. His research interests include wireless communications and networks, cyber physical systems, machine learning, and security. He has coauthored more than 100 journals and conference papers and seven authored books in these research topics.

A. Lee Swindlehurst (Fellow, IEEE) received the B.S. and M.S. degrees in electrical engineering from Brigham Young University (BYU) in 1985 and 1986, respectively, and the Ph.D. degree in electrical engineering from Stanford University in 1991. He was with the Department of Electrical and Computer Engineering, BYU, from 1990 to 2007. From 1996 to 1997, he held a joint appointment as a Visiting Scholar with Uppsala University and the Royal Institute of Technology, Sweden. From 2006 to 2007, he was on leave as the Vice President of Research with ArrayComm LLC, San Jose, CA, USA. Since 2007, he has been a Professor with the Electrical Engineering and Computer Science (EECS) Department, University of California at Irvine. From 2014 to 2017, he was a Hans Fischer Senior Fellow with the Institute for Advanced Studies, Technical University of Munich. His research interests include array signal processing for radar, wireless communications, and biomedical applications. He has over 400 publications in these areas. In 2016, he was elected as a Foreign Member of the Royal Swedish Academy of Engineering Sciences (IVA). He received the 2000 IEEE W. R. G. Baker Prize Paper Award, the 2006 IEEE Communications Society Stephen O. Rice Prize in the field of communication theory, the 2006, 2010, and 2021 IEEE Signal Processing Society's Best Paper Award, the 2017 IEEE Signal Processing Society Donald G. Fink Overview Paper Award, the Best Paper Award from the 2020 IEEE International Conference on Communications, and the 2022 Claude Shannon-Harry Nyquist Technical Achievement Award from the IEEE Signal Processing Society. He was the inaugural Editor-in-Chief of the IEEE JOURNAL OF SELECTED TOPICS IN SIGNAL PROCESSING.

Zhu Han received the B.S. degree in electronic engineering from Tsinghua University in 1997 and the M.S. and Ph.D. degrees in electrical and computer engineering from the University of Maryland, College Park, MD, USA, in 1999 and 2003, respectively.

From 2000 to 2002, he was an Research and Development Engineer with JDSU, Germantown, MD, USA. From 2003 to 2006, he was a Research Associate with the University of Maryland. From 2006 to 2008, he was an Assistant Professor with Boise State University, Boise, ID, USA. He is currently a John and Rebecca Moores Professor with the Electrical and Computer Engineering Department as well as the Computer Science Department, University of Houston, Houston, TX, USA. His main research interests include the novel game-theory related concepts critical to enabling efficient and distributive use of wireless networks with limited resources, wireless resource allocation and management, wireless communications and networking, quantum computing, data science, smart grids, and security and privacy. He has been an AAAS Fellow since 2019. He received the NSF Career Award in 2010, the Fred W. Ellersick Prize of the IEEE Communication Society in 2011, the EURASIP Best Paper Award for the *Journal on Advances in Signal Processing* in 2015, the IEEE Leonard G. Abraham Prize in the field of communications systems (Best Paper Award in IEEE JOURNAL ON SELECTED AREAS IN COMMUNICATIONS) in 2016, and several best paper awards in IEEE conferences. He is also the winner of the 2021 IEEE Kiyo Tomiyasu Award, for outstanding early to mid-career contributions to technologies holding the promise of innovative applications, with the following citation: "for contributions to game theory and distributed management of autonomous communication networks." He was an IEEE Communications Society Distinguished Lecturer from 2015 to 2018 and an ACM Distinguished Member since 2019. Since 2017, he has been a 1% Highly Cited Researcher according to Web of Science.

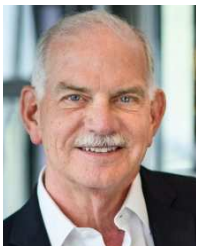

H. Vincent Poor (Life Fellow, IEEE) received the Ph.D. degree in EECS from Princeton University in 1977. He has also held visiting appointments at several other universities, including most recently the University of Berkeley and the University of Cambridge. From 1977 to 1990, he was on the faculty of the University of Illinois at Urbana–Champaign. Since 1990, he has been on the faculty of Princeton University, where he is currently the Michael Henry Strater University Professor. From 2006 to 2016, he was the Dean of the School of Engineering and Applied Science, Princeton University. His research interests include information theory, machine learning, and network science, and their applications in wireless networks, energy systems, and related fields. Among his publications in these areas is the recent book *Machine Learning and Wireless Communications* (Cambridge University Press, 2022). He is a member of the National Academy of Engineering and the National Academy of Sciences. He is a Foreign Member of the Chinese Academy of Sciences, the Royal Society, and other national and international academies. He received the IEEE Alexander Graham Bell Medal in 2017.